EFDA–JET–PR(10)12

P. Mantica, T. Tala, J.S. Ferreira, A.G. Peeters, A. Salmi, D.Strintzi, J. Weiland,
M. Brix, C. Giroud, G. Corrigan, V. Naulin, G.Tardini, K.-D.Zastrow
and JET EFDA contributors

Perturbative Studies of Toroidal Momentum Transport using NBI Modulation in JET: Experimental Results, Analysis Methodology and First Principle Modelling

Perturbative Studies of Toroidal Momentum Transport using NBI Modulation in JET: Experimental Results, Analysis Methodology and First Principle Modelling

P. Mantica[1], T. Tala[2], J.S. Ferreira[3], A.G. Peeters[4], A. Salmi[5], D. Strintzi[6], J. Weiland[7], M. Brix[8], C. Giroud[8], G. Corrigan[8], V. Naulin[9], G. Tardini[10], K.-D. Zastrow[8] and JET EFDA contributors*

JET-EFDA, Culham Science Centre, OX14 3DB, Abingdon, UK

[1]Istituto di Fisica del Plasma, EURATOM/ENEA-CNR Association, 20125, Milano, Italy
[2]Association EURATOM-Tekes, VTT, P.O. Box 1000, FIN-02044 VTT, Finland
[3]Associação EURATOM/IST, Centro de Fusão Nuclear, 1049-001 Lisbon, Portugal
[4]Centre for Fusion Space and Astrophysics, University of Warwick, Coventry 7AL, UK
[5]Association EURATOM-Tekes, Helsinki University of Technology, P.O. Box 2200, FIN-02150 TKK, Finland
[6]National Technical University of Athens, Association Euratom-Hellenic Republic, GR-15773 Athens, Greece
[7]Chalmers University of Technology and Euratom-VR Association, Göteborg Sweden
[8]EURATOM-CCFE Fusion Association, Culham Science Centre, OX14 3DB, Abingdon, OXON, UK
[9]Association Euratom-Risø DTU, DK-4000 Roskilde, Denmark
[10]Max-Planck-Institut für Plasmaphysik, EURATOM Association, Garching, Germany
** See annex of F. Romanelli et al, "Overview of JET Results", (Proc. 22 [nd] IAEA Fusion Energy Conference, Geneva, Switzerland (2008)).*

Preprint of Paper to be submitted for publication in
Physics of Plasmas

ABSTRACT.
Perturbative experiments have been carried out in the JET tokamak in order to identify the diffusive and convective components of toroidal momentum transport. The torque source was modulated either by modulating tangential neutral beam power or by modulating in anti-phase tangential and normal beams to produce a torque perturbation in the absence of a power perturbation. The resulting periodic perturbation in the toroidal rotation velocity was modelled using time dependent transport simulations in order to extract empirical profiles of momentum diffusivity and pinch. Details of the experimental technique, data analysis and modelling are provided. The momentum diffusivity in the core region ($0.2<\rho<0.8$) was found to be close to the ion heat diffusivity (χ_ϕ/χ_i~0.7-1.7) and a significant inward momentum convection term, up to 20m/s, was found, leading to an effective momentum diffusivity significantly lower than the ion heat diffusivity ($\chi_\phi^{eff}/\chi_i^{eff}$~0.4). These results have significant implications on the prediction of toroidal rotation velocities in future tokamaks and are qualitatively consistent with recent developments in momentum transport theory. Detailed quantitative comparisons with the theoretical predictions of the linear gyro-kinetic code GKW and of the quasi-linear fluid Weiland model are presented for two analyzed discharges.

1. INTRODUCTION

The study of plasma rotation and momentum transport in tokamaks is currently experiencing an intensive experimental and theoretical research effort, in view of extrapolating plasma performance from present devices to future machines like ITER. The role of sheared rotation in the quenching of turbulence with subsequent improvement in confinement [1-3] is well known, as well as the stabilizing effect of toroidal rotation on pressure limiting resistive wall modes [4]. The lower rotation expected as a consequence of lower torque and larger inertia may thus be detrimental for ITER performance. However, a reliable prediction of magnitude and profile of toroidal rotation in a device like ITER is presently still not possible, both because transport of toroidal momentum is less known than heat or particle transport, and because we lack a precise knowledge of all torque sources and plasma momentum self-generation processes. These reasons have led to the present intensification of research on momentum transport.

The momentum diffusivity χ_ϕ and pinch velocity v_{pinch} (negative sign denotes inwards) are related to the toroidal velocity v_ϕ, its gradient ∇v_ϕ and the momentum flux Γ_ϕ, assuming the absence of a significant particle flux, as follows:

$$\Gamma_\phi \sim -n\,\chi_\phi\,\nabla v_\phi + n\,v_{pinch}\,v_\phi = -n\,\chi_\phi^{eff}\,\nabla v_\phi \qquad (1)$$

where n is the ion density. It is always possible to combine the diffusive and convective part of the momentum flux into an effective momentum diffusivity χ_ϕ^{eff}, which can be calculated from steady-state rotation profiles once momentum sources are known. In the following the term "steady-state" will be used to indicate a quantity taken at a given time (or time averaged over a given interval),

therefore not resolving the modulation time dependence, whilst the term "stationary" will be used to indicate conditions where plasma parameters and profiles do not exhibit significant slow trends. On the theoretical side, substantial progress has been achieved in the understanding of momentum transport driven by Ion Temperature Gradient modes (ITGs)[5-10]. Fluid models and gyro-kinetic codes have been developed, which link inherently momentum and ion heat transport, foreseeing similar diffusivities for both channels (Prandtl number, $P_r = \chi_\phi/\chi_{\phi i} \sim 1$). In addition, the recently predicted existence of an inward momentum pinch is a qualitatively new ingredient in assessing the achievable rotation peaking in ITER, where torque sources will be located mainly in the outer regions. As found for particle transport, the impact of the pinch existence on the plasma profiles would be higher for momentum than for heat, for which the presence of an inward pinch, if any, is always dominated by the high diffusive transport component due to the core localization of heat sources.

On the experimental side, a significant improvement in the characterization of the steady-state behaviour of toroidal rotation has been achieved, both in plasmas with external torque source [11-14] and in plasmas without external torque sources [15-16], which still exhibit non-zero toroidal rotation, the so-called "intrinsic rotation", whose physical origin is still under investigation. A rather surprising recent observation from steady-state momentum studies is that the effective momentum diffusivity is much lower than the ion heat diffusivity ($P_r^{eff} = \chi_\phi^{eff}/\chi_i^{eff} \sim 0.4$ using the definition of χ_ϕ as in Eq.1)[11,13-14], apparently contradicting the theoretical expectations. It is clear that the existence of a momentum inward pinch would solve the apparent contradiction, allowing for similar diagonal diffusivities at the same time as different effective values. However, a direct demonstration of the existence of a momentum pinch is fairly difficult from steady-state data only. A clean way of identifying separately diffusive and convective transport components is by means of perturbative experiments [17], i.e. exploiting the additional information contained in the dynamic response of the plasma rotation to a time variation of the torque source. Modulation at a suitable frequency has the advantage of optimizing the S/N ratio by averaging over several cycles and has been used successfully to study electron and more recently ion heat transport, and also particle and impurity transport (see [18] for a recent review). Its application to momentum transport studies using Neutral Beam Injection (NBI) modulation is a recent development, with a couple of studies reported in JT-60U [19,20], one experiment reported in JET [21,22,23] and one in DIII-D [24]. The use of magnetic perturbations to brake the plasma was reported in DIII-D [25] and NSTX [24, 26, 27] as another means to induce a transient from which it is possible to infer diffusivity and convection separately.

This paper describes momentum perturbative experiments using Neutral Beam Injection (NBI) modulation at JET, presenting both new experiments and more refined analysis and modelling with respect to previous work [21,22,23] and including detailed comparison of the results with recent gyro-kinetic and fluid theory predictions. Sect.2 illustrates the experiments, Sect.3 discusses the calculations of the time dependent torque deposition, Sect.4 illustrates the rather heavy experimental methodology, based on transport modelling required to extract from the data the estimates of momentum diffusivity and pinch, Sect.5 summarizes the linear gyro-kinetic predictions, Sect.6 describes

first attempts to perform time-dependent modelling of the rotation dynamic response with 1D quasi-linear fluid transport models. Sect.7 summarizes the results and discusses future developments.

2. EXPERIMENTAL RESULTS

2.1. OUTLOOK OF EXPERIMENTAL SET-UP

The toroidal momentum perturbative experiments have been carried out in low collisionality JET H-mode plasmas ($B_T = 3$T, $I_p = 1.5$MA, $n_{e0} \sim 4\times10^{19}$ m^{-3}) with minimum level of MHD activity to prevent interference with the pertubation analysis, i.e. at high $q_{95} \sim 7$ to avoid large sawteeth in the centre and with type III ELMs to avoid large periodic edge crashes. Total power levels were up to 13MW for NBI and 4MW for ICRH in H minority scheme. In these conditions, ITGs are the dominant instability, making the coupling of momentum and ion heat transport, and thus the concept of Prandtl number, unambiguous. The NBI torque source is the best available tool on JET for inducing a significant rotation perturbation, although it is not ideal because its deposition profile is very broad, which is a complicating factor in the analysis, unlike in the case of localized RF heat sources. On the other hand, the torque sources from NBI can be calculated more precisely than radio-frequency power sources. Momentum transfer from the NBI fast ions to the thermal bulk plasma takes place via two main mechanisms [28]: a) passing ions transfer toroidal angular momentum to the bulk plasma by collisions, which is a slow process; b) trapped ions transfer their momentum by $\boldsymbol{J}\times\boldsymbol{B}$ forces, which is practically an instantaneous process ($\boldsymbol{J}$ denotes displacement current density due to finite banana orbit width and $\boldsymbol{B}$ magnetic field). The collisional torque dominates in the centre whilst the $\boldsymbol{J}\times\boldsymbol{B}$ torque dominates from mid-radius to the plasma edge. If the frequency of the modulation is fast enough compared to the fast ion slowing down time, the $\boldsymbol{J}\times\boldsymbol{B}$ component will dominate over the collisional one in the perturbation source. In the analysis both collisional and $\boldsymbol{J}\times\boldsymbol{B}$ torque have been taken into account. In the JET experiments, the NBI power and torque were square wave modulated with a duty cycle d.c.= 50% or 33% at a frequency f = 6.25Hz or 8.33Hz, which is the highest technically possible. Using the latter, $\boldsymbol{J}\times\boldsymbol{B}$ torque becomes the dominant source of torque perturbation. The modulation frequency is much slower than the 10ms time resolution of the Charge Exchange Recombination Spectroscopy (CXRS) diagnostic used to measure the toroidal rotation profile ω_ϕ and ion temperature T_i at 12 radial points [29]. Consequently, it is possible to observe changes in toroidal rotation in the beam on and beam off periods and perform the Fourier analysis of the modulated rotation. The modulation took place in a stationary phase for several seconds following two basic schemes:

1) torque modulation with non-compensated power modulation, modulating (80ms ON, 80ms OFF or 40ms ON, 80ms OFF) 3-4 tangential beams up to 6MW of modulated power. This technique is the most straightforward and allows a good S/N level in the toroidal rotation modulation. As discussed above, the perturbed torque source is the sum of the collisional and $\boldsymbol{J}\times\boldsymbol{B}$ torque delivered by each tangential beam. Time traces of NBI power, torque density at two radial locations as calculated by TRANSP [30] (see sect.3), toroidal angular rotation

frequency $\omega_\phi = v_\phi/R$ (R is the major radius), T_i and T_e at mid-radius for 9 of the modulation cycles are illustrated in Fig.1. Steady-state profiles of n_e, T_e, T_i , ω_ϕ, P_e, P_i and TRANSP calculated torque density are shown in Fig.2. All spatial information in the paper is provided using as radial coordinate the normalized toroidal radius, $\rho_{tor} = \rho_t/\rho_t^{edge}$ where $\rho_t = \sqrt{\Phi/\pi B_0}$, with F the toroidal magnetic flux, and ρ_t^{edge} is the value of ρ_t at the plasma boundary. One can see in Fig.1 the different time behaviour of the $\boldsymbol{J}\times\boldsymbol{B}$ and collisional torque, the first having the same square wave modulation as power, due to instantaneous deposition, the second being integrated by the fast ion slowing down time. A clear rotation modulation is visible in Fig.1. Due to the concomitant power modulation, also the electron and ion temperature are modulated, as well as the total energy content and plasma position, which are complications to be accounted for in the analysis, as discussed in sect. 2.2 and 4.1.2.

2) torque modulation with compensated power modulation, modulating in anti-phase 3 tangential and 3 normal beams (50ms ON tangential, 110ms ON normal). In this way there is no net power modulation, hence no temperature and plasma position modulation. The torque modulation also partly cancels, the remaining torque modulated component being due to the differences in torque deposition between tangential and normal beams. While beam particles absorbed at the high field side of magnetic axis become passing ions, those absorbed at the low field side become either passing or trapped ions depending on the inverse aspect ratio of the flux surface where they are created, $\varepsilon = r/R$. For the parameters of the so called normal neutral beams on JET, the fast ions are passing, i.e. $\xi = \frac{R_{imp}}{R} > \xi_t = \sqrt{\frac{2\varepsilon}{1+\varepsilon}}$ (where R_{imp} is the impact radius), for $\rho_{tor} = 0.24$, while for the tangential neutral beam bank they are passing for $\rho_{tor} = 0.39$. Therefore in a simplified picture, in the inner plasma region $0.24 < \rho_{tor} = 0.39$ the perturbed source will be dominated by the normal beams, whilst in an intermediate region outside $\rho_{tor} = 0.39$ there would be cancellation of the $\boldsymbol{J}\times\boldsymbol{B}$ component of normal and tangential beams, leaving further out a $\boldsymbol{J}\times\boldsymbol{B}$ component from tangential beams. The collisional torque component from tangential and normal beams should also to large extent cancel, decreasing its weight in comparison with the non-compensated case. Therefore this experiment should have resulted in a better spatial localization of the perturbed torque source, although with somewhat peculiar phasing, possibly allowing transport analysis in a source free region. However, as discussed more in detail in Sect.3 on the basis of the FFT of the TRANSP calculated torque, the actual torque cancellation was not complete, and in addition also the S/N of the rotation perturbation in these experiments turned out much lower, as can be seen from the time traces in Fig.3 (Fourier analysis is the only way to detect the rotation modulation). Fig.4 shows the steady-state profiles for this case. In conclusion this configuration did not deliver the anticipated advantages in spite of the additional complications of the experiment and has therefore been abandoned in our later experiments on JET.

2.2 FOURIER ANALYSIS OF ROTATION AND TEMPERATURE MODULATION AND CORRECTIONS FOR OSCILLATING PLASMA POSITION

Standard Fourier analysis (FFT) has been applied to the experimental time traces at various radial positions of ω_ϕ, T_i and T_e, to derive spatial profiles of amplitude (A) and phase (φ) of the perturbation at the 1st harmonic of the modulation frequency for d.c.=50% and also at the 2nd harmonic for d.c.=33%. The 3rd harmonic is always below noise level. The profiles are shown in Fig.5 for a non-compensated case at 6.25Hz, 50% d.c., in Fig.6 for a similar shot with non-compensated modulation at 8.33Hz , 33% d.c. and in Fig.7 for a compensated case at 6.25Hz, 33% d.c. For the first non-compensated case also the temperature perturbations are shown, whilst for the compensated case the temperature perturbation is null. Phase values are always calculated with respect to the phase of the tangential beam power. The statistical error bars are calculated for the amplitudes from the noise level outside the spectral peaks and for the phases by assuming that the noise level would add up to the signal with a 90^o phase shift (worst case).

As mentioned in Sect.2.1, in the non-compensated case the plasma equilibrium changes periodically with the modulated NBI power. This is important as the experimental CXRS data is measured at fixed positions in the laboratory frame, resulting in a spurious measured ω_ϕ, T_i and T_e oscillation due to the oscillating equilibrium, which would falsify the transport analysis if not properly taken into account. Rotation and temperature must therefore be properly mapped into a plasma movement independent radial co-ordinate system before performing the transport analysis and modelling. Here, this is done within TRANSP using the time dependent EFIT reconstructed equilibrium constrained by Motional Stark Effect measurements to map all experimental data onto the same flux surface grid used for the torque calculation and the transport simulations. Both horizontal and vertical plasma oscillations are taken into account. The outcome of the correction procedure is illustrated in detail in Fig.5a-b, where the corrected A and φ profiles are shown by dashed lines and compared to uncorrected values in Fig.5a for ω_ϕ and in Fig.5b for T_i. The details of T_e modulation are not important for the following analysis and modelling, so only the uncorrected data is shown for sake of information. The effect of oscillating displacement is found rather important on T_i oscillations but minor on ω_ϕ oscillations. The data in Fig.6 are already corrected. This correction is obviously not needed in the compensated case.

It can be noted in Fig.5a that the rotation perturbation A and φ profiles are highly influenced by the non-localized source profiles, made by two different components with a time shift, rather than by transport processes only, at variance with most perturbative heat transport experiments. In fact the amplitude is maximum in the centre, corresponding to the collisional torque source which is dominant there at 6.25Hz, but the phase is minimum around ρ~0.6, which is the region of the instantaneous $\boldsymbol{J}\times\boldsymbol{B}$ torque deposition. The increase in φ towards the centre is not only due to propagation of the $\boldsymbol{J}\times\boldsymbol{B}$ rotation wave, but also to the high phase values associated to the fast ion slowing down that provides the central collisional torque source. This is a clear indication that, due to the non-localization of the modulated torque source, a simple determination of the momentum

diffusivity and pinch directly from the spatial derivatives of the amplitude and phase of the modulated ω_ϕ is not viable. Therefore, time-dependent transport modelling of ω_ϕ is required to extract the transport properties from the plasma dynamic response, assuming that torque sources are known with reasonable accuracy from numerical calculations.

Figure 7 illustrates the measured A and φ for the compensated experiment. The results are in line with the expectation of a much narrower torque source in the centre, since at mid-radius ($0.3<\rho_{tor}<0.7$), there is a zone of partial cancellation between normal and tangential beams. However, a priori we would have expected a much clearer separation of normal and tangential peaks in the amplitude profiles (see discussion on torque source in Sect.3.1). The transition from normal to tangential torque component is clearly visible in the large increase of phase between $\rho_{tor} = 0.2$ (where normal beams dominate) and $\rho_{tor} = 0.7$ (where tangential beams dominate, although with much smaller amplitudes), due to the 180^o phase jump in the torque of the two sources. The very external region ($\rho_{tor}>0.8$) is again dominated by normal beams, as can be seen from the increase of amplitudes in the region $\rho_{tor}>0.8$, with the same phasing of the normal beams. This could be due to a larger deposition of trapped particles in the external region by the normal beams. This region ($\rho_{tor}>0.8$) is outside the scope of this paper which focuses on core momentum transport. Also TRANSP torque calculations become less reliable in this region where the plasma profiles are not known with similar accuracy as in the core.

3. NUMERICAL COMPUTATION OF THE TIME DEPENDENT TORQUE SOURCE

3.1 POWER AND TORQUE CALCULATIONS USING TRANSP AND ASCOT

Due to the absence of a source free region where the transport analysis could be done independently of the details of the source, the calculation of the time dependent torque profile is an essential step for the derivation of the momentum transport coefficients from the data. The transport analysis will in fact rely on full transport simulations in which the source is inputted as known, with the obvious consequence that any error in the source will determine an error on the derived transport coefficients. Great care has then been dedicated to such torque calculations and associated uncertainties.

The TRANSP code [30] has been used to calculate NBI power and torque profiles as a function of time, given the time dependent experimental profiles of all plasma parameters, but neglecting the small temporal oscillations of plasma parameters due to the NBI modulation itself, to avoid polluting with noise the main torque oscillation coming from the NBI oscillating waveform. T_i has been taken from CXRS, T_e from ECE radiometer and LIDAR, n_e from interferometer and LIDAR, Z_{eff} from CXRS and spectroscopic measurements. Error bars are typically ±5% for T_i and T_e, ±10% for n_e, ±20% for Z_{eff}. The internal TRANSP equilibrium solver with EFIT data as boundary condition was used to calculate equilibrium consistently with the slow time variations of profiles. The fast equilibrium variations due to modulation have been neglected because as discussed in Sect.2.2 their effect has been removed from the data before they are compared with simulations. TRANSP contains the NUBEAM Monte Carlo solver [31], which has always been used with a high number

(160 000) of particles. A test of the sensitivity of torque amplitudes and phases to the number of Monte Carlo particles has shown that in excess of 80000 particles are needed to reach convergence in the results. The torque calculations are reliable up to $\rho_{tor} = 0.8$, due to uncertainties in the plasma parameters in the external region.

Figure 8 shows A and φ of the NBI total torque density and of the ion and electron power densities calculated for shot 66128. The steady-state torque density for this shot was already shown in Fig.2. The central torque density perturbation is typically in the order of 10% whilst the central power density perturbation is ~3%. One can notice the zero-phase, instantaneous torque deposition for $\rho_{tor}>0.4$ due to the $\boldsymbol{J\times B}$ torque, whilst in the central region the main torque component is the delayed collisional one. The ion and electron power phases also indicate collisional deposition from fast NBI ions to thermal population, with longer collisional times to ions than to electrons. Fig.9 shows A and φ of the calculated torque density for Pulse No: 73701, at two harmonics of the modulation frequency, indicating separately the $\boldsymbol{J\times B}$ and collisional components. In this shot due to higher modulation frequency (8.33Hz rather than 6.25Hz of Pulse No: 66128), the $\boldsymbol{J\times B}$ torque dominates at all radii but the very central region.

In order to gain confidence in the correctness of the TRANSP NUBEAM calculations, the modulated torque for 73701 has been calculated also with the orbit following ASCOT code [32]. ASCOT is similar to NUBEAM module within TRANSP. Both codes are guiding centre following MC codes with internal NBI birth profile generator. In ASCOT calculations the small temporal variations in equilibrium due to the NBI modulation are neglected and a constant EFIT reconstructed equilibria with MSE constraint are used together with time averaged plasma profiles. Time varying NBI waveforms provide the dynamics in torque profiles. The results for A and φ are shown in Fig.10, again indicating the $\boldsymbol{J\times B}$ and collisional components. Fig.11 compares the steady-state torque density calculated with TRANSP and ASCOT. The agreement between the two very different and independent codes is remarkable and constitutes the most powerful confirmation that we can rely on the torque calculations for our transport analysis.

Finally, the A and j of modulated torque density for the compensated case, Pulse No: 73700, are shown in Fig.12 calculated with TRANSP and in Fig.13 calculated with ASCOT, and indicating separately the $\boldsymbol{J\times B}$ and collisional components. To help visualization of the complex torque dynamics, in Fig.14 we also show the A and φ of the torque density calculated with ASCOT indicating separately the normal and tangential beams. The phase is always taken with respect to the tangential beams. One can see that the peak in A of the perpendicular beams is shifted slightly inside with respect to the one of the tangential beams, and the two are in phase opposition, so that there is a partial cancellation leading to a more narrow total deposition (with respect to the non-compensated case) dominated by the perpendicular beams in the central region. However at the frequency used (6.25Hz) there is still a significant central collisional component that comes mainly from the tangential beams. Moreover, the fact that the cancellation in the external region is not perfect, leads to the impossibility of considering such region as source free for the analysis,

which in practice vanifies the usefulness of this approach, as will be discussed in detail in Sect.4.2.

3.2 ANALYSIS OF SENSITIVITY TO PLASMA PARAMETERS

Having assessed by comparing two different codes the reliability of the torque calculations for a given set of plasma parameters and profiles, in this section we deal with the assessment of uncertainties in torque following from uncertainties in plasma parameters. We have evaluated the impact of the most important players, i.e. n_e, T_e, Z_{eff}. The ***J×B*** torque is essentially instantaneous and depends only on the initial deposition (governed by n_e and Z_{eff} to lesser extent). T_e and Z_{eff} affect the slowing down rate and ion to electron heating ratio and thus the torque deposition dynamics. T_i is not a very sensitive player as it has practically no role in the initial deposition and only affects the ion slowing down at low energies, but has no effect on electron slowing down and thus its overall effect on torque dynamics is usually small. Of course, additionally, NBI acceleration voltage and beam fractions play a role but these can be assumed to be known.

Figure 15 shows the variation of A and j of the torque density when a) n_e is varied between 0.8 and 1.2 of the experimental value, b) T_e is varied between 0.8 and 1.2 of the experimental value, c) Z_{eff} is decreased from the experimental value of 1.9 to 1. Once can see that the impact is only on amplitudes, not on phases. As we will discuss in the next sections, this implies that the momentum diffusivity, or Prandtl number, is a robust quantity, insensitive to errors in plasma parameters. The pinch value, instead, depends on the torque amplitudes and therefore its determination will be affected by larger uncertainties, reflecting those in the measured plasma parameters. Amongst these, the main impact is given by density, with a variation of about ±15% when n_e is varied in an interval ±20% of the measured value. T_e and Z_{eff} have much smaller impact. Particular care has then to be paid in assessing the best n_e profile. For the LIDAR measurements used in this paper the uncertainty on n_e is ±10% and this has been further improved following the recent introduction of n_e measurements using High Resolution Thomson Scattering (Δn_e~±5%). Therefore, we do not expect uncertainties larger than ±4-8% in torque profiles associated to uncertainties in plasma parameters.

4. TRANSPORT ANALYSIS OF TIME DEPENDENT TOROIDAL ROTATION USING JETTO

4.1 THE NON-COMPENSATED MODULATION CASE

4.1.1 Empirical transport model with diffusivity constant in time

The power and torque sources calculated by TRANSP and described in Sect.3 have been used in the transport analysis of toroidal rotation using the 1.5D code JETTO [33]. The transport equation for ω_ϕ is solved while q-profile, T_i, T_e and n_e are frozen to their experimental values. The boundary conditions for steady-state ω_ϕ, amplitudes $A(\omega_\phi)$ and phases $\varphi(\omega_\phi)$ of the modulated ω_ϕ are chosen to fit the experimental data at $\rho = 0.8$ as the edge plasma transport is beyond the scope of interest in this study. The transport simulations for shot 66128 are carried out over the 9 modulation cycles shown in Fig.1.

The transport model for toroidal momentum is an empirical one, constant in time, featuring a

diagonal momentum diffusivity given by $\omega_\phi = P_r \cdot \chi_{i,}^{eff}$ (where P_r is the Prandtl number and $\chi_{i,}^{eff}$ the effective ion heat diffusivity, which is a good estimator of the diagonal $\chi_{i,}$ because there is no experimental evidence of an ion heat pinch in JET from existing T_i modulation experiments [34,35]) and a pinch velocity v_{pinch}. The values of P_r and v_{pinch} are chosen in such a way that they fit the available data with sufficient accuracy according to visual inspection (in principle their profiles are completely free with no outside constraints).

The simulations are run with 3 logical steps: 1) run a fully interpretative simulation to calculate $\chi_{i,}^{eff}$; 2) run predictive simulations for ω_ϕ varying the P_r value and profile until a reasonable reproduction of the experimental phase profile of the modulated ω_ϕ is obtained, as the phase is rather insensitive to v_{pinch}; 3) vary v_{pinch} value and profile to reproduce also the amplitude of the modulated ω_ϕ and its steady-state profile. Step 1 is straightforward as $\chi_i^{,eff}$ can be calculated from the measured T_i data and calculated power deposition profiles. $\chi_{i,}^{eff}$ is shown in Fig.16. Step 2 leads to a rather precise identification of the acceptable range of P_r values, since P_r is the only unknown (the sources are taken from the NUBEAM calculations). This resolves the indeterminacy associated with the analysis of only the steady-state profile, as the latter can be reproduced by an unlimited number of possible combinations for χ_ϕ and v_{pinch} yielding the same $\chi_{\phi,}^{eff}$. Once P_r is identified, step 3 allows us to identify also the convective component that enables us to reproduce the steady-state ω_ϕ and amplitude with the chosen P_r. As an initial choice, P_r was taken uniform along radius, and as a refinement, P_r has been chosen to have a radial profile, as suggested from the gyro-kinetic simulations described in Sect.5, but most of all because it provides a better fit to most of the shots analyzed.

In Figs. 17 we show the simulations of the modulated data of Pulse No: 66128 corresponding to the two most obvious options for χ_ϕ(i.e. P_r) and v_{pinch}: in Fig.17a we fix P_r=0.5 to yield $\chi_\phi \approx \chi_{\phi,}^{eff}$ and v_{pinch}= 0 whilst in Fig.17c we follow the above described best-fit procedure, which leads to P_r~2 as the best value to fit the phase profiles, and to the v_{pinch} profile shown in Fig.16, with values up to 20 m/s, to fit amplitudes as well as steady-state. It can be seen in Fig.17b that both simulations predict the steady-state ω_ϕ within 10% accuracy in the region of interest, i.e. $0.2<\rho_{tor}<0.8$. Inside ρ_{tor} <0.2, neo-classical transport starts to dominate ion heat transport, and the predictions are worse as the use of the ITG based P_r for calculating ω_ϕ is not appropriate. In figure 17a and 17c one can see that the two options differ in reproducing the $A(\omega_\phi)$ and $\varphi(\omega_\phi)$ profiles. The case with P_r = 0.5 and v_{pinch}= 0 clearly disagrees with the experiment. The simulated phase is too large inside and this is an indication of too low χ_ϕ, i.e. too low P_r used in the simulation. On the other hand, the simulated amplitude is too low towards the plasma centre, which could only be cured by lowering χ_ϕ further. This shows that a model with v_{pinch} = 0 is not compatible with the experimental data. In the second case, the agreement between the simulated and experimental amplitudes and phases improves dramatically. Using P_r = 2 the χ_ϕ is now large enough to yield perfect match of the phase profile, and the pinch is required to provide the observed amplitude peaking. This is a direct indication of the existence of a convective term in the toroidal momentum transport. The same simulation using, instead of uniform P_r, a radially varying P_r profile as shown in Fig.16, and with the same v_{pinch} gives

in this case as good agreement with experimental A and φ as the $P_r = 2$ simulation (Fig.17d), but a better steady-state rotation profile. A sensitivity analysis using the experimental uncertainties on A and φ and on plasma parameters and torque source shows that the range of P_r and v_{pinch} values compatible with such uncertainties is in the range of 20–30%, outside which the simulated phase, amplitude and steady-state deviate unacceptably from the experimental values.

Another example is the simulation of Pulse No: 73701 (two harmonics available), shown in Fig18. This has been simulated using the same procedure and the profiles of χ_ϕ and v_{pinch} derived from the best fit procedure are shown in Fig.19. Again, a high P_r number and a significant pinch are required to fit the experimental data.

4.1.2 Effect of fluctuating χ_i due to T_i oscillations

A significant complicating factor in the non-compensated experiment is the T_i modulation induced by the NBI power modulation. In fact, being the ITG the supposed drive of toroidal momentum transport, a time varying T_i and/or R/L_{Ti} implies a time varying ITG driven transport, both for ion heat and momentum. The induced oscillation in χ_ϕ produces a component in the rotation modulation, adding an extra contribution to the $A(\omega_\phi)$ and $\varphi(\omega_\phi)$ profiles, which, if not properly taken into account, may lead to an erroneous evaluation of the P_r and v_{pinch} values. Therefore it is important to assess quantitatively the relevance of this mechanism on the results of Sect.4.1.1.

As seen in figure 5b-c for Pulse No: 66128, the ion and electron temperatures are modulated with peak amplitudes around 70eV, i.e. a perturbation of ~1%, while the modulation amplitude in ω_ϕ is around 4%. To estimate the impact of such T_i modulation on the determined P_r and v_{pinch}, a time-dependent χ_i has been calculated for Pulse No: 66128 using the CGM model based on the critical gradient length concept [36]. This model has no implications on momentum transport and here it has been used only to evaluate the expected modulation in χ_i (and through P_r in χ_ϕ) because it is a model commonly used in JET to investigate ion heat transport from T_i modulation experiments [34,35]. Typical values for ion threshold and stiffness found in JET in shots similar to the ones discussed here have been used to model the modulated T_i and the associated time variation of χ_i and χ_ϕ. The reason why we did not use directly the time dependent experimental χ_i^{eff} instead of the one modelled by CGM is the very high level of noise that is fed into to the experimental χ_i^{eff} by the experimental determination of the T_i gradient. Fig.20 shows the time traces of χ_i at different radii, Fig.21a the simulated T_i modulation and Figs.21b-c the ω_ϕ modulation, with the same two assumptions for P_r and v_{pinch} as in Figs.17b-d. One can see that the reproduction of T_i modulation in Fig.21a is satisfactory, given the large uncertainties associated with the T_i modulation data after subtraction of the oscillating displacement effect, which for T_i is significant, as was shown in Fig.5b. This allows us to assume that the level of oscillation of χ_i in Fig.20 is representative of the amount of effect to be expected, even if we cannot have a precise determination of threshold and stiffness level for this shot. One can also see that the simulations of ω_ϕ with oscillating χ_i (and consequently χ_ϕ) in Figs. 21b-c do not differ significantly from their counterparts with constant χ_i in Figs.17b-d. One can conclude that, owing to

the small amplitude of the T_i modulation and of the induced χ_i and χ_ϕ modulation, the effect on the values determined for P_r and v_{pinch} is insignificant. The same conclusion is actually derived from the first principle simulations using the quasi-linear fluid Weiland model [37] discussed in Sect.6.

4.2 THE COMPENSATED MODULATION CASE

The same procedure described in Sect.4.1.1 has been applied to the compensated modulation case, Pulse No: 73700, using the TRANSP time dependent torque described in Sect.3. In this case the logic behind the best-fit is however completely different, because it is no longer true that phases are uniquely determined by diffusivities. In fact, best-fitting the data has turned out very cumbersome, because the phase profile is the result of two propagating waves (normal and tangential beams) of modulated rotation, in anti-phase with each other, so that the amplitude of each component plays a dominant role in determining the resultant phase, and therefore momentum pinch enters in the phase dynamics as well. The core being dominated by the normal beams, whilst the outer region by the tangential, the rapidity of the increase by 180^o of the phase between the two components depends crucially on the Prandtl number: low P_r number yields a very fast transition, whilst high P_r number a smooth one, with the pinch value determining the precise phase profile. In addition, a low P_r number would yield two very well defined peaks of amplitudes, whilst a high P_r number would tend to smooth them down. It is clear from the data shown in Fig.7 that experimentally the transition is very smooth, and there is no pronounced peak of the tangential component, which are non trivial confirmations of the presence of a high P_r number (implying then a pinch in order to match the steady-state). The best simulation achieved for the compensated Pulse No: 73700 is compared against data in Fig.22 and shows a fair agreement in profile and magnitude for modulated and steady-state data. The P_r numbers and pinch profiles used in the simulation are shown in Fig.23. We conclude that the compensated modulation supports the previous conclusions about the existence of a pinch. In general, however, this procedure has turned out too cumbersome to be used for a systematic study of several shots such as when performing parametric scans. In addition, we note that the S/N level in such compensated modulation is much lower than in the non-compensated case, as amplitudes are reduced due to compensation. In particular outside $r = 0.5$, which is the region where the pinch is expected to be largest, the signal is very near to noise level, so the sensitivity of this technique to the pinch value is reduced. Since on the other hand the problem of modulated power is not found to seriously affect the data of the non-compensated case, as discussed in Sect.4.1, the compensated technique has been abandoned at JET and the non-compensated one has been used for further studies of parametric dependencies of momentum transport, which will be the object of a future paper.

5. THEORETICAL PREDICTIONS OF TOROIDAL MOMENTUM TRANSPORT FROM LINEAR GYROKINETIC SIMULATIONS

Effective transport of momentum needs, like all turbulent transport, a phase shift between the turbulent velocity fluctuations and the momentum fluctuations. Such a phase shift is established by

a finite average rotation but also generally through symmetry breaking, in which case residual stresses or asymmetry momentum fluxes arise [6,8]. For negligible residual stress terms, the resulting equation for the transport of momentum can be directly written as the sum of a diffusive and pinch contribution in the local limit. Off diagonal terms, i.e. a momentum flux directly driven by the density and temperature gradients,†have been investigated in global simulations in [38] and were found to be†one order smaller in normalized Larmor radius and †therefore negligible for JET parameters.

Gyro-kinetic studies of the diffusion coefficient c_f are presented in [6,9], whereas the pinch term v_{pinch} was derived in [7] using the co-moving reference frame (for more details on the derivation see [39]). In the co-moving frame the toroidal rotation enters the equations only through the Coriolis drift velocity. Consequently, any toroidal momentum pinch is directly related to the Coriolis drift. Since this drift, unlike the drifts due to the magnetic field inhomogeneity, is linear in the parallel velocity, it generates a coupling between density / temperature perturbations and the perturbations in the parallel velocity. Over this coupling the temperature perturbations of the ITG generate parallel velocity perturbations that are then transported by the $\boldsymbol{E}\times\boldsymbol{B}$ velocity leading to a finite radial flux of parallel momentum. Furthermore, the drift in the electrostatic potential perturbations accelerates the particles and also leads to the generation of parallel velocity fluctuations and consequently to a momentum flux. Although no complete expression for the flux has been derived for the laboratory frame, the latter effect is related to the turbulent equipartition (TEP [40]) theory and has recently been worked out in Ref. [8]. Obviously, the calculated radial fluxes should be frame independent and it can be shown that the TEP contribution is incorporated in the description that uses the Coriolis drift (see [41]).

The gyro-kinetic flux tube code GKW [42] is used here to calculate the values of the momentum transport coefficients under experimental conditions. All parameters are taken directly from the experiment, but the following approximations have been made: a) the geometry is approximated using the s-α model, with the circular radius chosen such that the number of trapped particles is roughly equal to the experimental case; b) a pure Deuterium plasma is considered and Coulomb collisions are neglected. The latter approximation is motivated by the small influence of the collisions [43]. The simulations presented here have been performed for the most unstable mode $k_\theta\rho_s = 0.3$.

The P_r number (χ_ϕ / χ_i) and the pinch number (Rv_{pinch}/χ_ϕ) profiles calculated by GKW are compared with the experimental ones in Fig. 24 and 25 for the JET Pulse No's: 66128 and 73701 respectively. The determination of both Prandtl number and pinch require two simulations per radial position: one with zero rotation ($v_\phi = 0$) and one with zero gradient (grad $v_\phi = 0$). In the latter case the diagonal contribution is zero, and hence the momentum flux, which is obtained from the code directly, gives the pinch contribution ($v_{pinch} = \Gamma_\phi / n\, v_\phi$), whereas in the former case the pinch contribution is zero and the momentum flux gives information on the diffusion coefficient ($\chi_\phi = -\Gamma_\phi / n\, \mathrm{grad} v_f$). Of course, this procedure assumes that the fluxes are linear in both v_f and grad v_f, an assumption that is well satisfied as shown in [7].

One can see that for Pulse No: 73701 (low density) the predicted and experimental Prandtl and

pinch numbers are in excellent agreement with experiment. However in Pulse No: 66128 (higher density) experimentally the reduction in χ_i due to increased density is larger than the one in χ_f, thus giving origin to higher experimental P_r and pinch numbers, whilst the theory prediction remains basically unchanged. Therefore a discrepancy by a factor 1.5-2 is present in this latter shot between GKW estimates and experiment. This seems a trend with density which however will be further investigated with more shots in a future work. On the other hand, the theoretical description of momentum transport is still evolving and at present it may already be quite satisfactory to find an agreement with experiment within a factor 2. Indeed more than one reason can be put forward. Nonlinear effects, for instance, might lead to different transport coefficients. Furthermore, several effects, like the ***E×B*** shearing [44], the current symmetry breaking [45], the residual stress [46] are not kept in the current description.

Finally we remark that with linear simulations only normalized quantities can be compared with experiment, but not absolute values of transport coefficients. This will have to wait for non-linear gyro-kinetic simulations of momentum transport. This observation justifies the attempt made in the next section to compare with experiment the predictions of the quasi-linear fluid Weiland model, which can be used for a full transport simulation of the time evolution of rotation, thereby allowing a complete comparison with experiment.

6. TIME DEPENDENT FLUID MODELLING

This section describes first attempts to do time dependent simulations of the JET NBI modulation experiments using the quasi-linear toroidal drift wave fluid model described in Ref. [37], which due to the inclusion of a space dependent nonlinear frequency shift (giving zonal flows) is no longer quasi-linear, in which a new treatment of momentum transport has been recently implemented [10]. New aspects are the inclusion of stress tensor effects for the toroidal momentum [7-10]. As it turns out, toroidal effects from the stress tensor [7] are important for the parallel ion motion which we here use as an approximation for the toroidal motion. The toroidal curvature effects enter both for the diagonal and convective parts of the momentum transport:

$$m\left[\frac{\partial}{\partial t} + (v_E + 2v_D)\cdot\nabla\right] v_{||} = e\left[E_{||} + (\vec{v}\times\vec{B})_{||}\right] - \frac{1}{n} e_{||}\cdot\nabla P - \frac{1}{n}\nabla\cdot\Pi_{off} \qquad (1)$$

Here the diagonal contributions from the stress tensor were included explicitely but the off- diagonal contributions are still kept in the remaining part Π_{off} of the stress tensor. The diagonal element of the toroidal momentum transport becomes [7,10]:

$$\chi_\phi = \frac{\gamma^3/k^2}{(\omega_r - 2\omega_{Di})^2 + \gamma^2} \qquad (2)$$

The convective fluxes are here taken from the kinetic formulation in [8]. The same fluxes have, however, recently been derived from a fluid formulation in [10]. They are divided into Turbulent

Equipartition (TEP) [8,41]

$$\Gamma_{tep} = \mathrm{Re}\{\ \frac{<k_{||}> c_s^2 - V_{||0}\bar{\omega}_{De}}{\omega - 2\bar{\omega}_{Di}}\ \hat{\phi} v_{Er}^{*}\} \tag{3}$$

and thermodiffusion

$$\Gamma_{term} = \mathrm{Re}\left\{\frac{<k_{||}> c_s^2 - V_{||0}\bar{\omega}_{De}}{\omega - 2\bar{\omega}_{Di}}\ \frac{\delta p}{\tau p} v_{Er}^{*}\right\} \tag{4}$$

The magnetic drift frequency has here been averaged over the mode profile as indicated by the bar in $\bar{\omega}_{Di}$. Moreover $<k_{||}>$ has been averaged over the radial mode profile. It is nonzero due to symmetry breaking effects of flowshear and magnetic curvature. The expression is quite complicated and given in Ref. 10. The curvature parts of (3,4) usually dominate except close to marginal stability.

Since the diagonal element for the ion thermal conductivity is obtained from (2) by replacing 2 in the denominator by 5/3 we realize that the Prandtl number of the diagonal components has to be very close to 1. Of the new convective parts, the thermodiffusion is usually the dominant part and is also usually directed inward. As compared to a model without the toroidal stress tensor effects, both diagonal and convective fluxes are considerably larger in the present model. Although the steady state sometimes does not change very much with the new model, the transient transport does.

This model has been used for 1.5D transport simulations of the JET Pulse No's: 66128 and 73701 (non compensated NBI modulation cases) described previously. Time dependent simulations were carried out by predicting $\omega_{\phi,}$ T_i, T_e and keeping n_e fixed to the experimental time-averaged steady-state values. Fig.26 shows the rotation steady-state (a) and modulation A and φ (b) for Pulse No: 66128, comparing the experiment with the simulation. Fig.26c shows for the same simulation the profiles of T_i and T_e at a given time. Fig.27 shows radial profiles of turbulent χ_i (not including the neoclassical component) diagonal and effective (the simulation in fact foresees the existence of an ion heat pinch), of momentum diffusivity, χ_ϕ, diagonal and effective, and of momentum convective velocity v_{pinch} predicted by the model. For comparison also the experimental $\chi_{\phi i}^{eff}$ and χ_ϕ diagonal and v_{pinch} are plotted. We note that in the model the diagonal χ_i and also χ_ϕ (Eq.(2)) depend on the eigenfrequency. Through that they depend also on other gradients and thus their definition as diagonal elements is not really appropriate. This may be particularly important for this model where diagonal and effective ion thermal conductivities differ significantly. In Fig.28 the P_r and pinch number from the simulation (both defined using the diagonal diffusivities for $\chi_\phi$and χ_i) and from experiment (where we use the diagonal χ_ϕ but the effective χ_i since so far we have no experimental evidence of an ion heat pinch) are compared. Figures 29-31 show the same quantities (excluded the T_i and T_e profiles) for Pulse No: 73701. One can see that for both shots the model predicts the existence of a momentum pinch, however quantitatively in absolute magnitude significantly smaller than found in experiment (v_{pinch}~3-7 m/s in simulations against v_{pinch}~10-20 m/s in experiment). Also the absolute value of the diagonal χ_ϕ is significantly smaller in the simulations, which gives origin to steeper

simulated phase profiles in Figs.26 and 29. So in spite of a good agreement with experiment of steady-state rotation profiles and amplitudes, the disagreement on the phases clearly indicates that both momentum diffusivity and pinch are too low. Interestingly, the P_r and pinch number are not far off with respect to experiment, because χ_i, χ_ϕ and v_{pinch} are all too low, and their ratios remain close to the experimental ones (and to the GKW ones). This shows clearly that it is not sufficient to compare only dimensionless ratios to validate a model, but we need also the absolute values of the diffusivities. This is thus a question of overall normalization of the transport, a question which has not been addressed by the GKW results. We remark that also for the Weiland model as for GKW the agreement is better at low density, where the P_r number matches the experimental one at least in the inner part of the plasma (with a different, rather flat profile of P_r number, at variance with GKW), whilst at high density the experimental P_r number is well above the simulated one.

CONCLUSIONS

This paper describes in detail the technique set-up at JET to perform perturbative studies of momentum transport using NBI modulation. Experimentally the simplest method of square wave modulation of 4−5MW of NBI power has turned out the most robust to be used in future studies. It gives a good S/N for the rotation modulation, and complicating effects associated to power modulation (such as modulated plasma displacement and modulated ion heat transport) have been shown small and can in any case be accounted for in the analysis. The idea of compensating the power modulation by modulating in anti-phase normal and tangential beams yields a much poorer S/N, requires a rather cumbersome fitting procedure of the data and was shown to be less sensitive to the pinch value in the region of interest.

The method set-up for extracting the toroidal momentum diffusivity and pinch values is a full time-dependent simulation of a number of NBI modulation cycles using the JETTO code, with empirically adjusted profiles of Prandtl number and pinch in order to fit both the steady-state rotation profiles and amplitudes and phases at two harmonics of the rotation modulation. The key for the uniqueness of the result is that phases are dominantly sensitive to P_r number, whilst amplitudes and steady-state also to the pinch. The main source of uncertainty in the analysis is represented by the need of assuming the torque deposition profile from numerical computations. Therefore a lot of effort has been dedicated to sensitivity studies of the time-dependent torque calculations using TRANSP-NUBEAM Monte Carlo code. A comparison with the time dependent torque calculated by a totally independent tool , the orbit following Monte Carlo code ASCOT, has given further confidence on the reliability of the calculated torque source. An overall uncertainty of ~20% on Prandtl number and ~30% on pinch value has been estimated.

The physics results yielded by the analysis of NBI modulation data have provided valuable insight into momentum transport, allowing to solve the apparent discrepancy between the low effective momentum diffusivity (P_r^{eff}~0.4) measured in steady-state experiments, and the ITG based theory prediction of a P_r number close to 1. In fact, it is clear from the phase response to the modulation that the diagonal momentum diffusivity is fairly large (P_r~1-2) and that the low effective

diffusivity is due to the presence of a significant momentum pinch (v_{pinch} up to 20m/s in the outer part of the plasma). This finding on one hand is in very good qualitative agreement with the recent theory developments described in Sect.5 and 6, on the other hand it opens interesting perspectives for the possibility of having peaked rotation profiles also in machines with low torque input, allowing to exploit the beneficial effects of flow shear.

For this reason the experimental results for two shots have been compared with linear gyro-kinetic predictions of P_r number and pinch number using the code GKW. In addition, the full time evolution of the rotation during several modulation cycles has been computed with the recently updated quasi-linear Weiland model for momentum transport and compared with steady-state, amplitude and phase profiles. The GKW theoretical predictions are in very good agreement with data both in value and profile shape for the lower density shot, whilst the higher density shot has a larger experimental P_r number than predicted by theory. The reason for the high experimental P_r number is that the increasing density reduces χ_i more than χ_φ, in experiment, thereby inducing a significant variation of P_r number. The theory predicted P_r number is instead rather insensitive to variations in main plasma parameters. The reason for such discrepancy remains to be investigated with further experiments at varying plasma parameters such as density, collisionality and safety factor. Future work will also address the dependence of the momentum pinch on plasma parameters in both experiment and theory. We note also that linear simulations do not yield absolute values of diffusivity and pinch, so it is not possible to compare quantitative predictions of transport with data until non-linear simulations are available. This is the reason why full simulations of the data using the Weiland model have been attempted. This is presently the only fluid model that has incorporated recent theoretical advances in momentum transport. The main result is that although the dimensionless P_r and pinch number are rather similar to the GKW values and to experiment, the absolute values of χ_i , χ_φ and pinch are all too low compared to experiment, thereby yielding steeper profiles of amplitude and phases. Another observation is that the P_r profile is rather flat in the Weiland model, whilst the experimental and GKW ones are increasing with radius. These modeling results indicate that further work is needed towards the validation of a physics based model for momentum transport to be used for extrapolation to future devices.

ACKNOWLEDGEMENTS

This work, supported by the European Communities under the contract of Association between EURATOM/ENEA-CNR, was carried out within the framework of the European Fusion Development Agreement. The views and opinions expressed herein do not necessarily reflect those of the European Commission.

REFERENCES

[1]. H. Biglari, P.H. Diamond, P. Terry, Physics of Fluids B **2**, 1 (1990)
[2]. R.L. Miller *et al*., Physics of Plasmas **1**, 2835 (1994)
[3]. K.H. Burrell, Physics of Plasmas **4**, 1499 (1997)

[4]. A.M. Garofalo *et al*., Nuclear Fusion **41**, 1171 (2001)
[5]. B. Coppi, Nuclear Fusion **42**, 1 (2002)
[6]. A.G. Peeters and C. Angioni, Physics of Plasmas **12**, 072515 (2005)
[7]. A.G. Peeters, C. Angioni, D.Strintzi, Physics Review Letters **98**, 265003 (2007)
[8]. T.S. Hahm *et al*., Physics of Plasmas **14**, 072302 (2007)
[9]. D. Strintzi, A.G. Peeters, J. Weiland, Physics of Plasmas **15,** 044502 (2008)
[10]. J. Weiland *et al*., Nuclear Fusion **49**, 065033 (2009)
[11]. D. Nishijima *et al*., Plasma Physics Controlled Fusion **47**, 89 (2005)
[12]. J.S. de Grassie *et al*., Nuclear Fusion **43**, 142 (2003)
[13]. P.C. de Vries *et al.,* Plasma Physics Controlled Fusion **48**, 1693 (2006)
[14]. P.C. de Vries *et al*., Nuclear Fusion **48,** 065006 (2008)
[15]. J.E. Rice *et al*., Nuclear Fusion **47**, 1618 (2007)
[16]. L.-G. Eriksson *et al*., Plasma Physics Controlled Fusion **51,** 044008 (2009)
[17]. A.Jacchia *et al.,* Physics of Fluids B **3**, 3033 (1991)
[18]. P. Mantica, F.Ryter, C.R. Physique **7**, 634 (2006)
[19]. K. Nagashima *et al.,* Nuclear Fusion **34**, 449 (1994)
[20]. M. Yoshida *et al*., Nuclear Fusion **47**,†856 (2007)
[21]. T. Tala *et al*., Physics Review Letters **102**, 075001 (2009)
[22]. G. Tardini *et al*., Nuclear Fusion **49,** 085010 (2009)
[23]. T. Tala *et al*., Plasma Physics Controlled Fusion **49** B291-B302 (2007).
[24]. W.M. Solomon *et al*., Physics of Plasmas **17**, 056108 (2010)
[25]. W.M. Solomon *et al*., Nuclear Fusion **49,** 085005 (2009)
[26]. W. M. Solomon *et al.,* Physics Review Letters **101,** 065004 (2008)
[27]. S.M. Kaye *et al.,* Nuclear Fusion **49,** 045010 (2009)
[28]. K.-D Zastrow. *et al*., Nuclear Fusion **38**, 257 (1998)
[29]. C.R. Negus *et al*., Review Scientific Instruments **77**, 10F102 (2006)
[30]. R.J. Goldston *et al*., Computer Physics **43,** 61 (1981)
[31]. A. Pankin *et al*., Computer Physics Communication **159**, 157 (2004)
[32]. J.A. Heikkinen, S.K. Sipilä, Physics of Plasmas 2, 3724 (1995)
[33]. G. Cenacchi *et al*., JETTO: A free boundary plasma transport code (basic version) Rapporto ENEA RT/TIB 1988(5) (1988)
[34]. P. Mantica *et al*., Physics Review Letters **102**, 175002 (2009)
[35]. F. Ryter et al., *Simultaneous Analysis of Ion and Electron Heat Transport by Power Modulation in JET,* in Fusion Energy 2008 (Proc. 22nd Int. Conf. Geneva, 2008), EX/P5-19, IAEA, Vienna.
[36]. X. Garbet *et al*., Plasma Physics Controlled Fusion **46**, 1351 (2004)
[37]. J. Weiland, *Collective Modes in Inhomogeneous Plasmas*, IOP (2000)
[38]. A.G. Peeters *et al*., Plasma Physics Controlled Fusion **48,** B413 (2006)
[39]. A.G. Peeters *et al*., Physics of Plasmas **16,** 042310 (2009)
[40]. M.B. Isichenko, A.V. Gruzinov and P.H. Diamond, Physics Review Letters **74,** 4436 (1996)
[41]. A.G. Peeters *et al*., Physics of Plasmas **16,** 034703 (2009)
[42]. A.G. Peeters *et al*., Computer Physics Communication 180, 2650 (2009)
[43]. A.G. Peeters *et al*., Physics of Plasmas **16,** 062311 (2009)

[44]. R.R. Dominguez, GM Staebler, Physics Fluid B **5**, 3876 (1993)
[45]. Y. Camenen *et al.*, Physics Review Lettetters **102**, 125001 (2009)
[46]. P.H. Diamond *et al.*, Physics of Plasmas **15**, 012303 _2008.

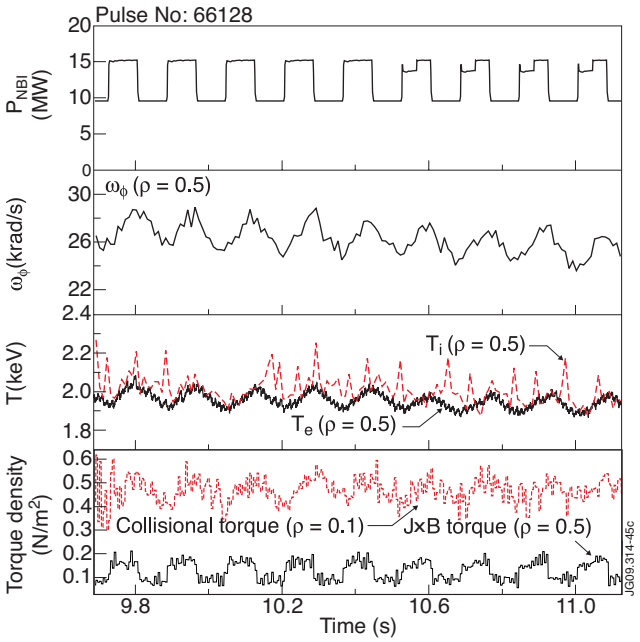

Figure 1: Time traces of the modulated NBI power, ω_ϕ, T_i and T_e and the two different components of the torque density for JET Pulse No: 66128 (non-compensated case).

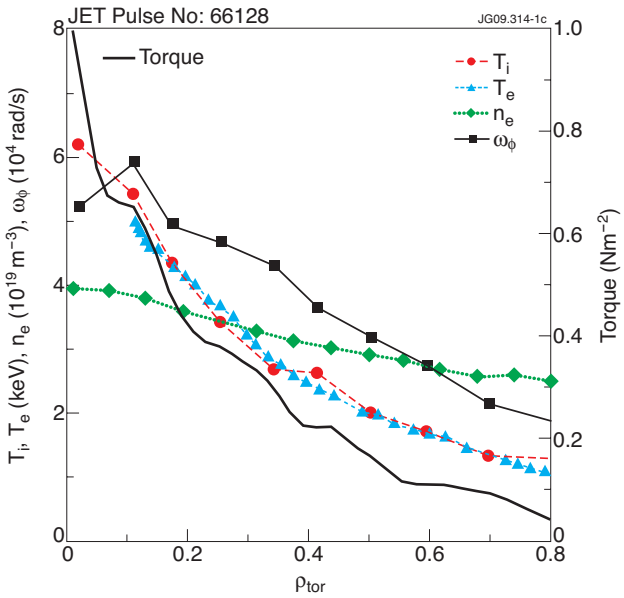

Figure 2: Steady-state radial profiles at t = 10s of ω_ϕ, T_i, T_e, n_e, and torque density for JET Pulse No: 66128.

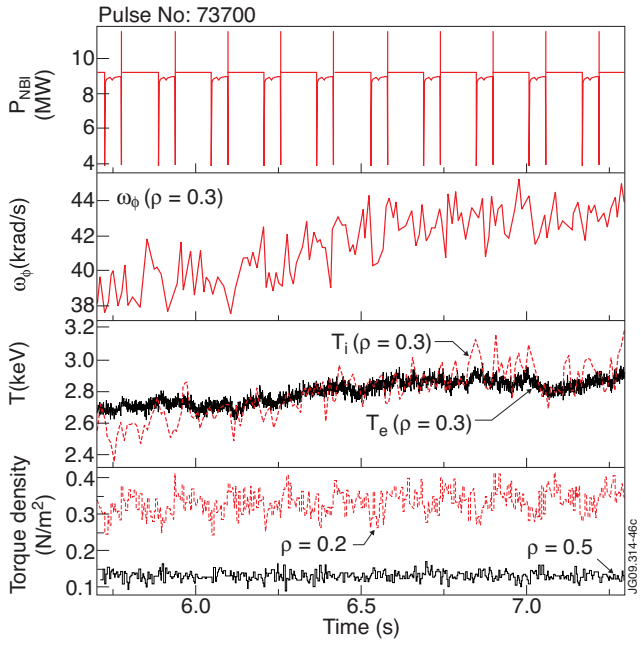

Figure 3: Time traces of the total NBI power, ω_ϕ, T_i and T_e at $\rho = 0.3$ and the total torque density at $\rho = 0.2$ and $\rho = 0.5$ for JET Pulse No: 73700 (compensated case).

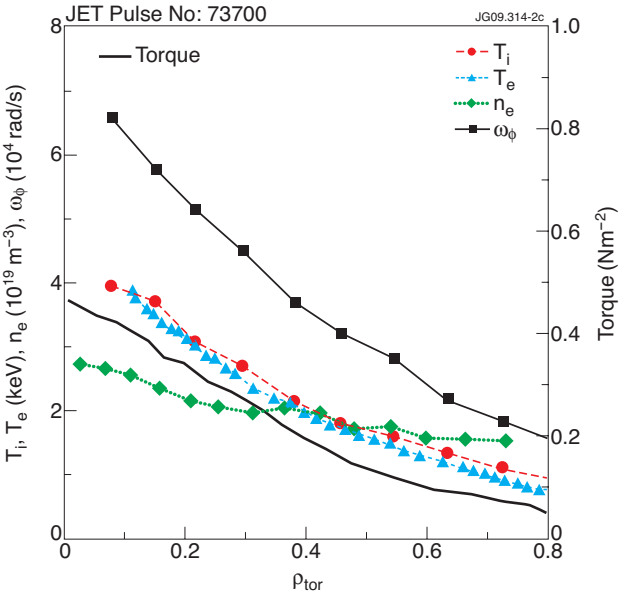

Figure 4: Steady-state radial profiles at t = 6.1s of ω_ϕ, T_i, T_e, n_e and torque density for JET Pulse No: 73700.

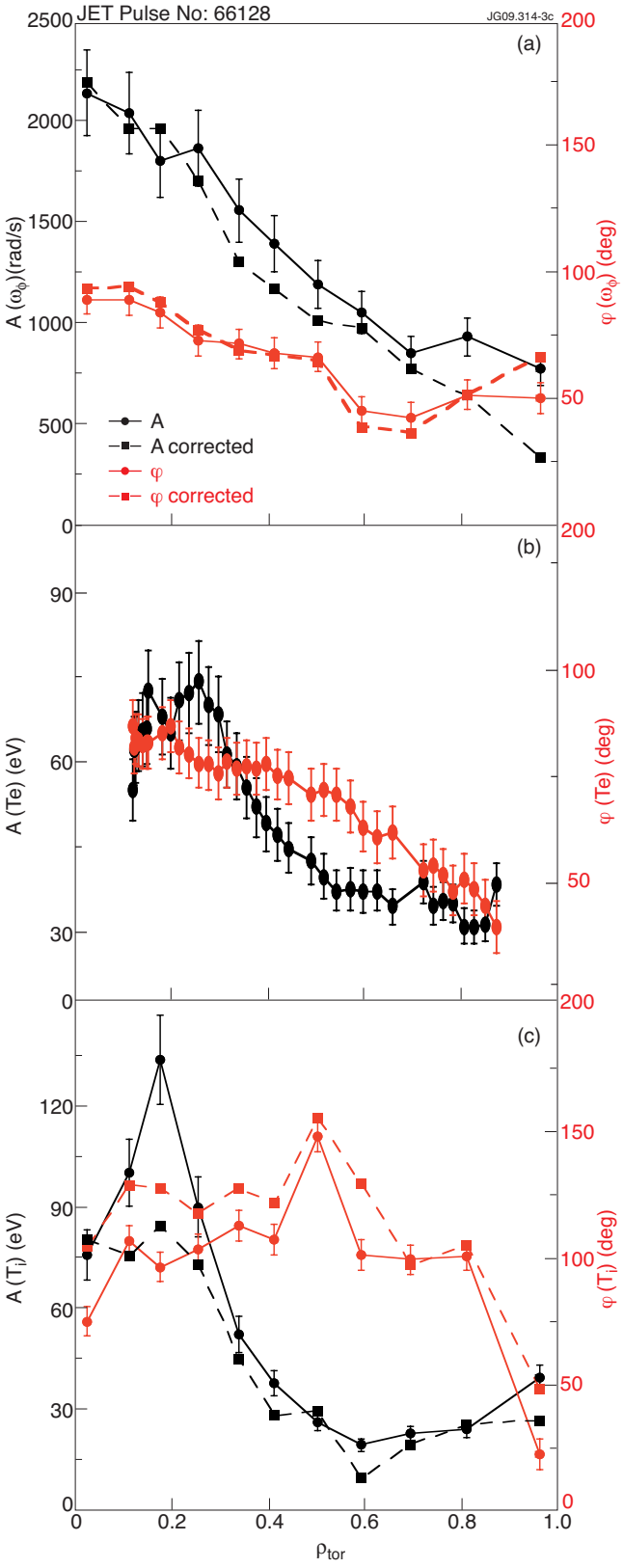

Figure 5: Radial profiles of A and φ at 6.25Hz in Pulse No: 66128 for: a)ω_ϕ, b) T_e, c) T_i . In a) and c) the data corrected for oscillating plasma position are shown.

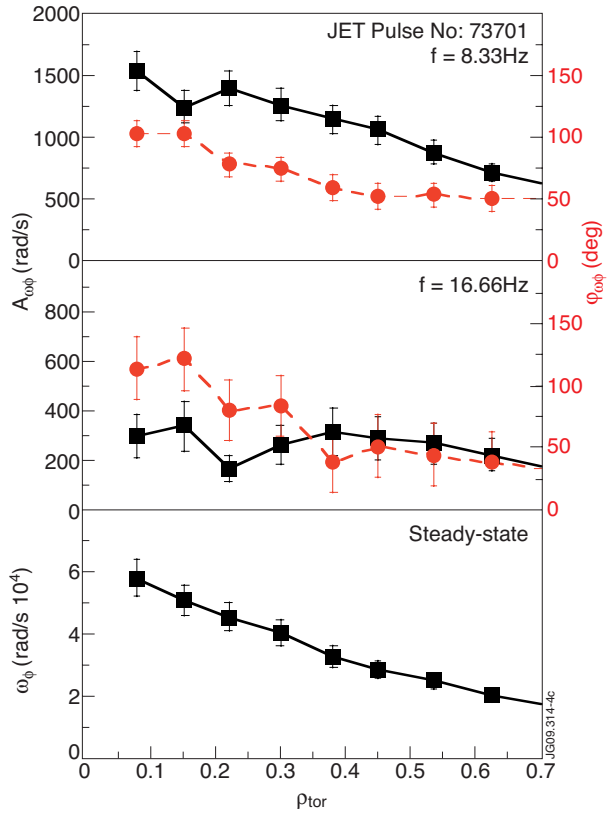

Figure 6: Radial profiles of A (black squares) and φ (red circles) at 8.33Hz and 16.66Hz and steady-state ω_ϕ in Pulse No: 73701.

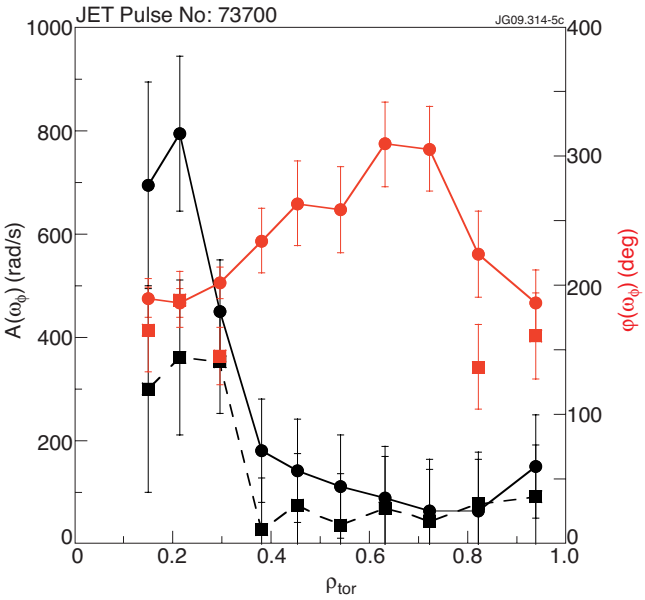

Figure 7: Radial profiles of A (black) and φ (red) of ω_ϕ at 6.25Hz (circles) and 12.50Hz (squares) in Pulse No: 73700 (compensated case). Phase values are not shown for 2nd harmonic at locations where amplitudes are below noise level.

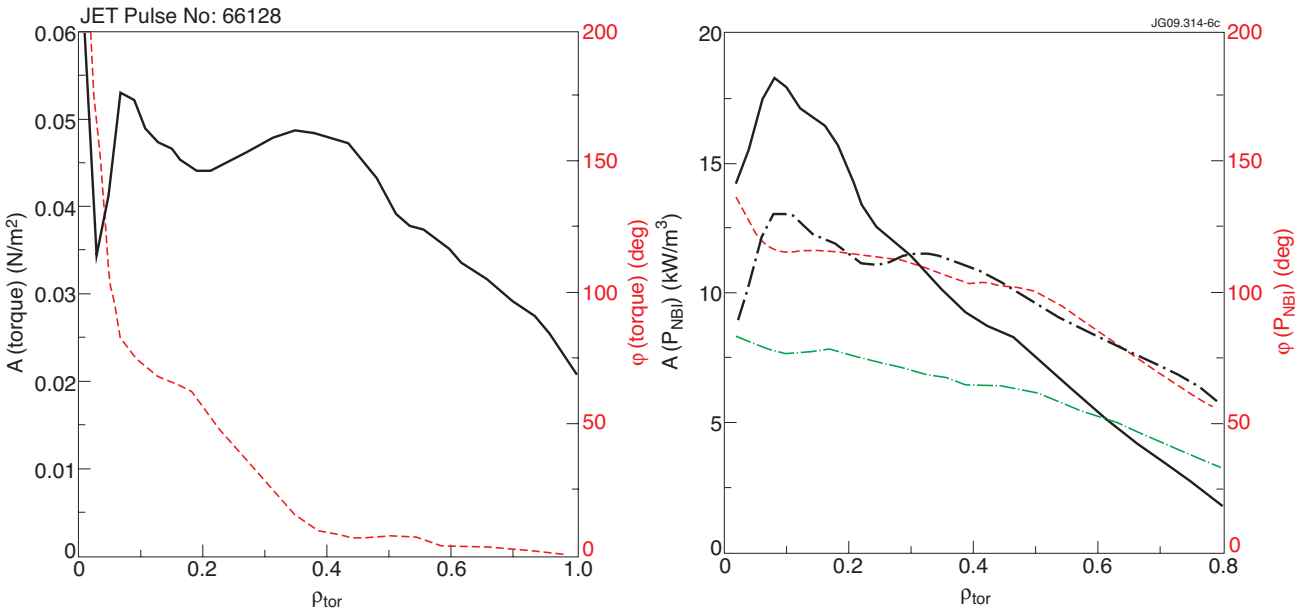

Figure 8: Radial profiles of A and φ at 6.25Hz in Pulse No: 66128 (non-compensated) for TRANSP calculated : a) total torque density (black full line: A, red dashed line: φ), b) on l(black full line: A, red dashed line: φ) and electron power density (grey dashed-dotted line: A, green dashed line: φ).

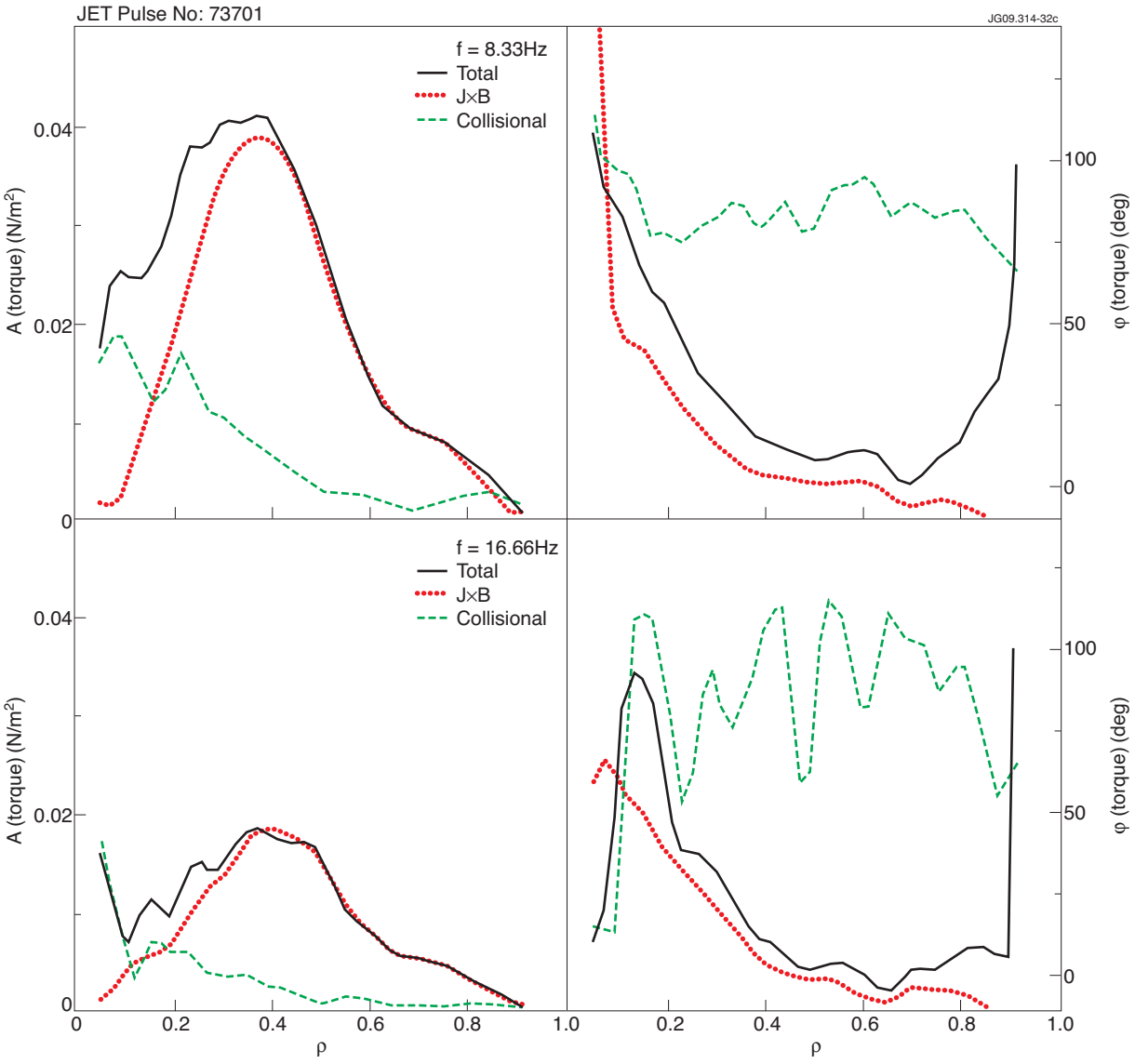

Figure 9: Radial profiles of A and φ of TRANSP calculated torque density at 8.33 and 16.66Hz in Pulse No: 73701 (non-compensated), distinguishing collisional and ***J×B*** *components.*

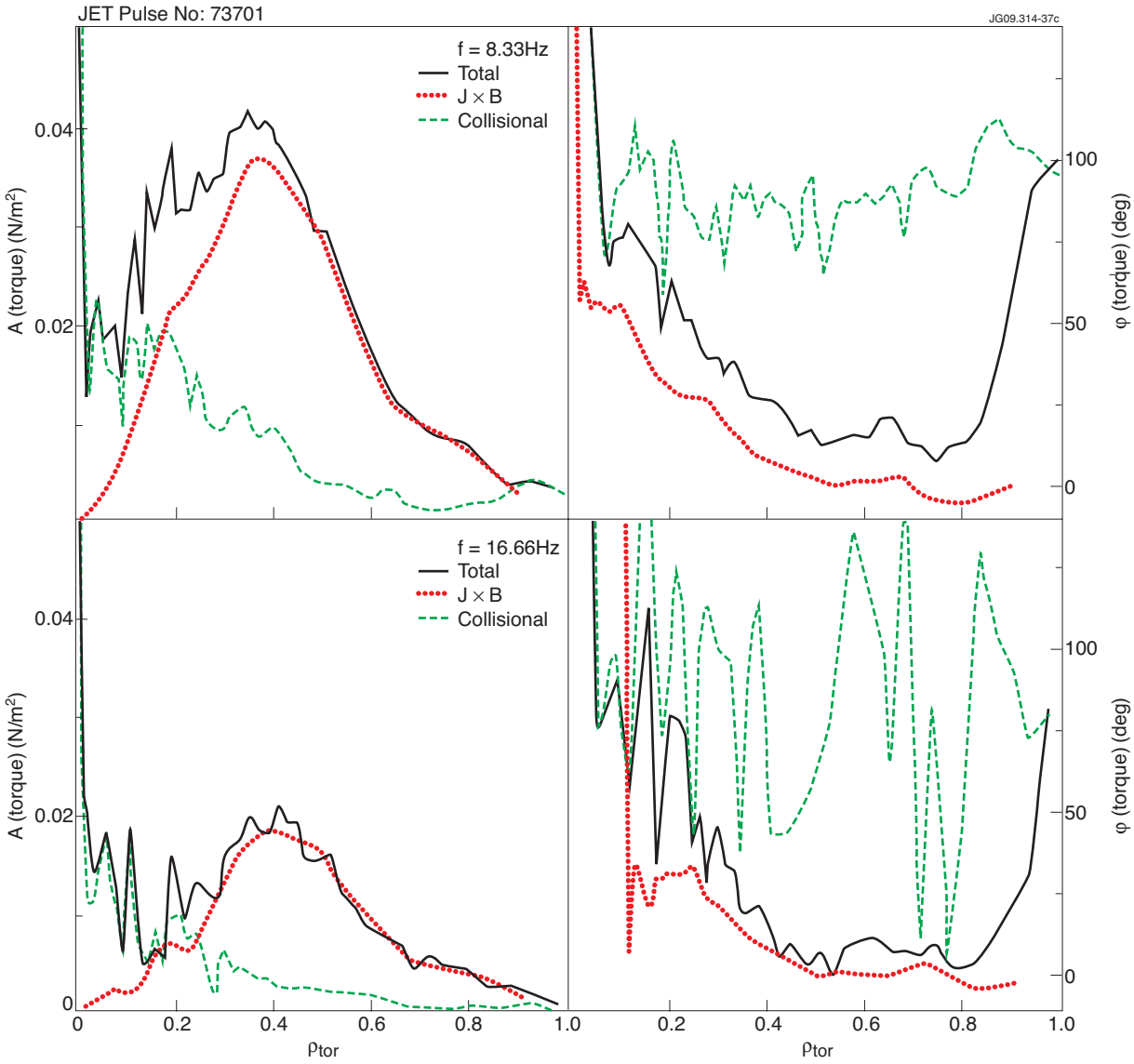

Figure 10: Radial profiles of A and φ of ASCOT calculated torque density at 8.33 and 16.66Hz in Pulse No: 73701 (non-compensated), distinguishing collisional and ***J×B*** *components.*

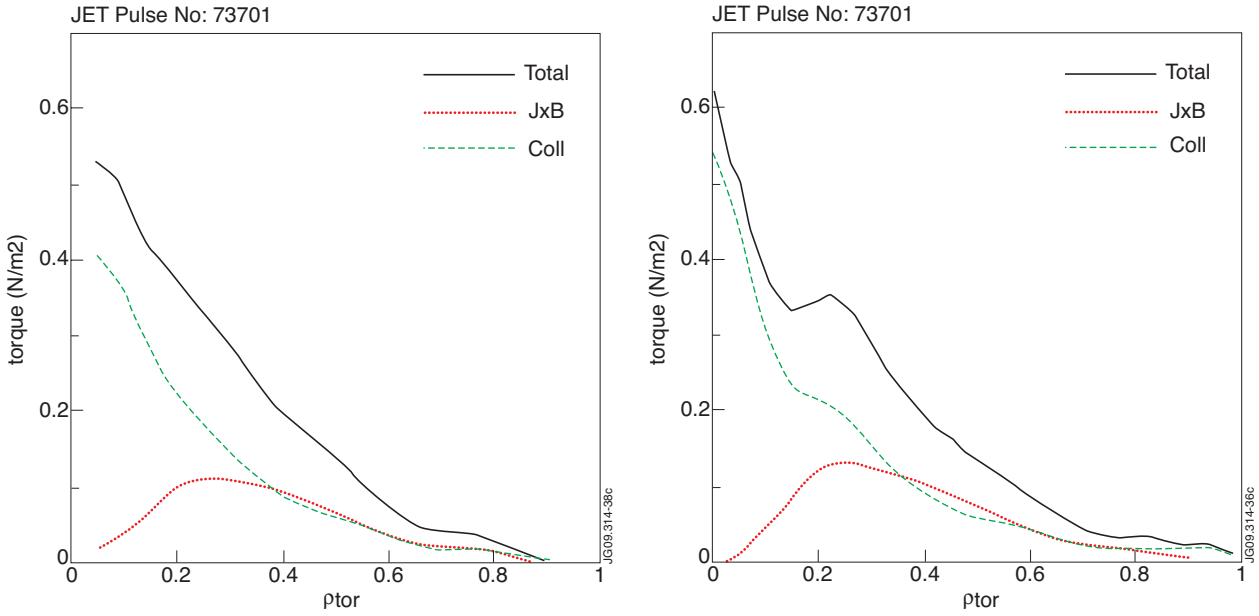

*Figure 11: Radial profiles of steady-state torque density in Pulse No: 73701 (non-compensated), distinguishing collisional and **J×B** components, calculated by (a) TRANSP, (b) ASCOT.*

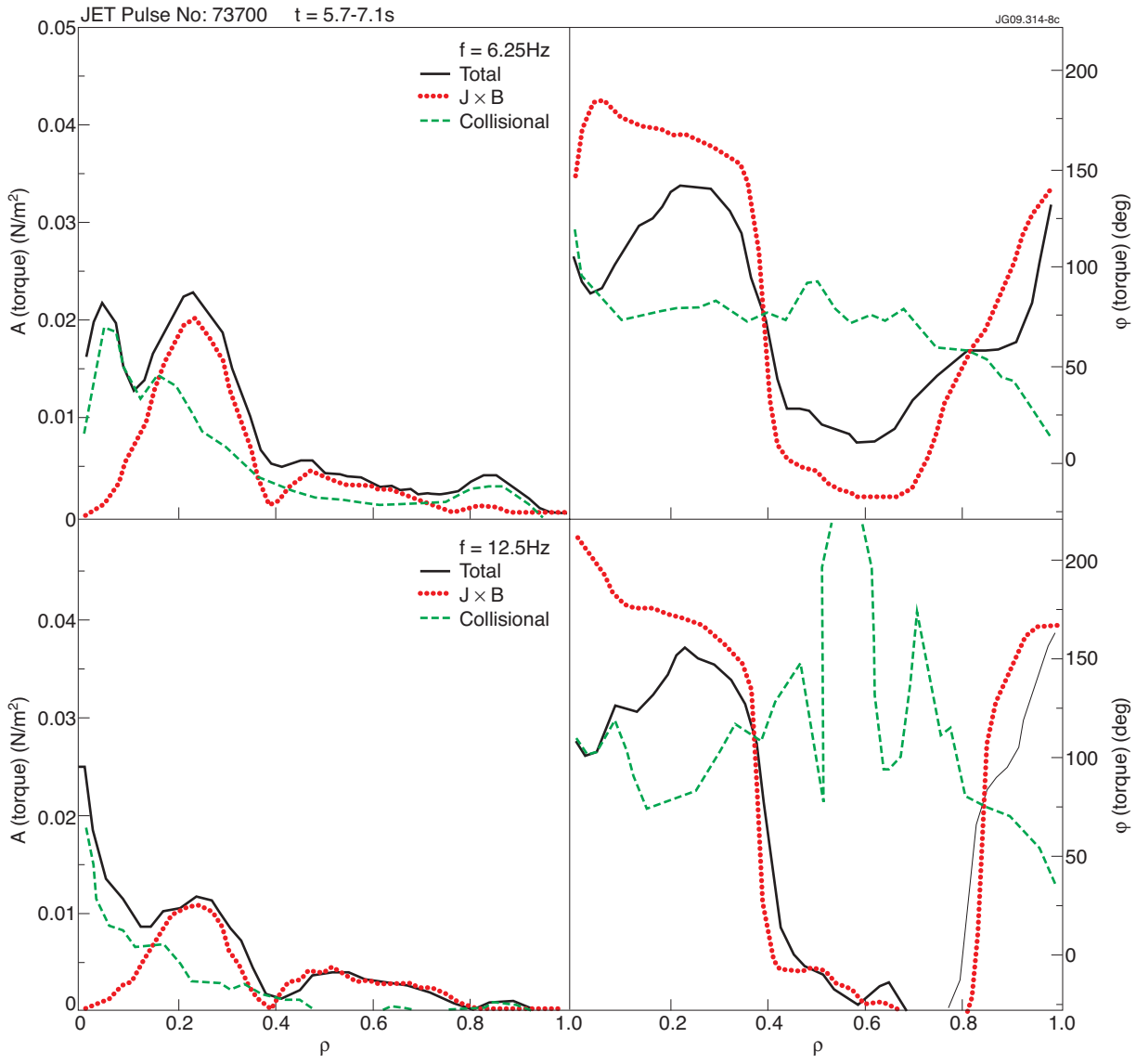

*Figure 12: Radial profiles of A and φ of TRANSP calculated torque density at 6.25 and 12.5Hz in Pulse No: 73700 (compensated), distinguishing collisional and **J×B** components.*

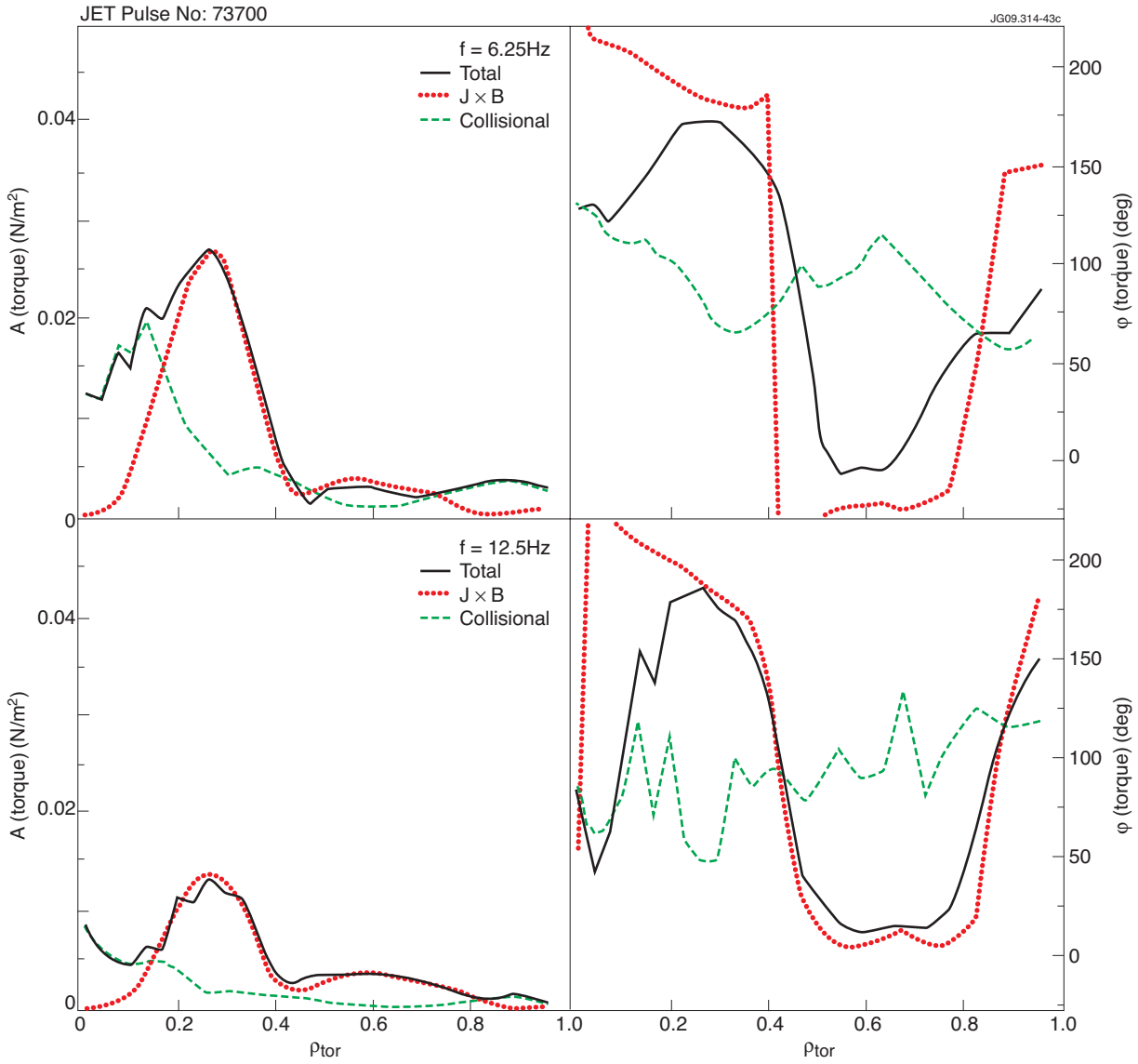

*Figure 13: Radial profiles of A and φ of ASCOT calculated torque at 6.25 and 12.5Hz in Pulse No: 73700 (compensated), distinguishing **J×B** and collisional beam components.*

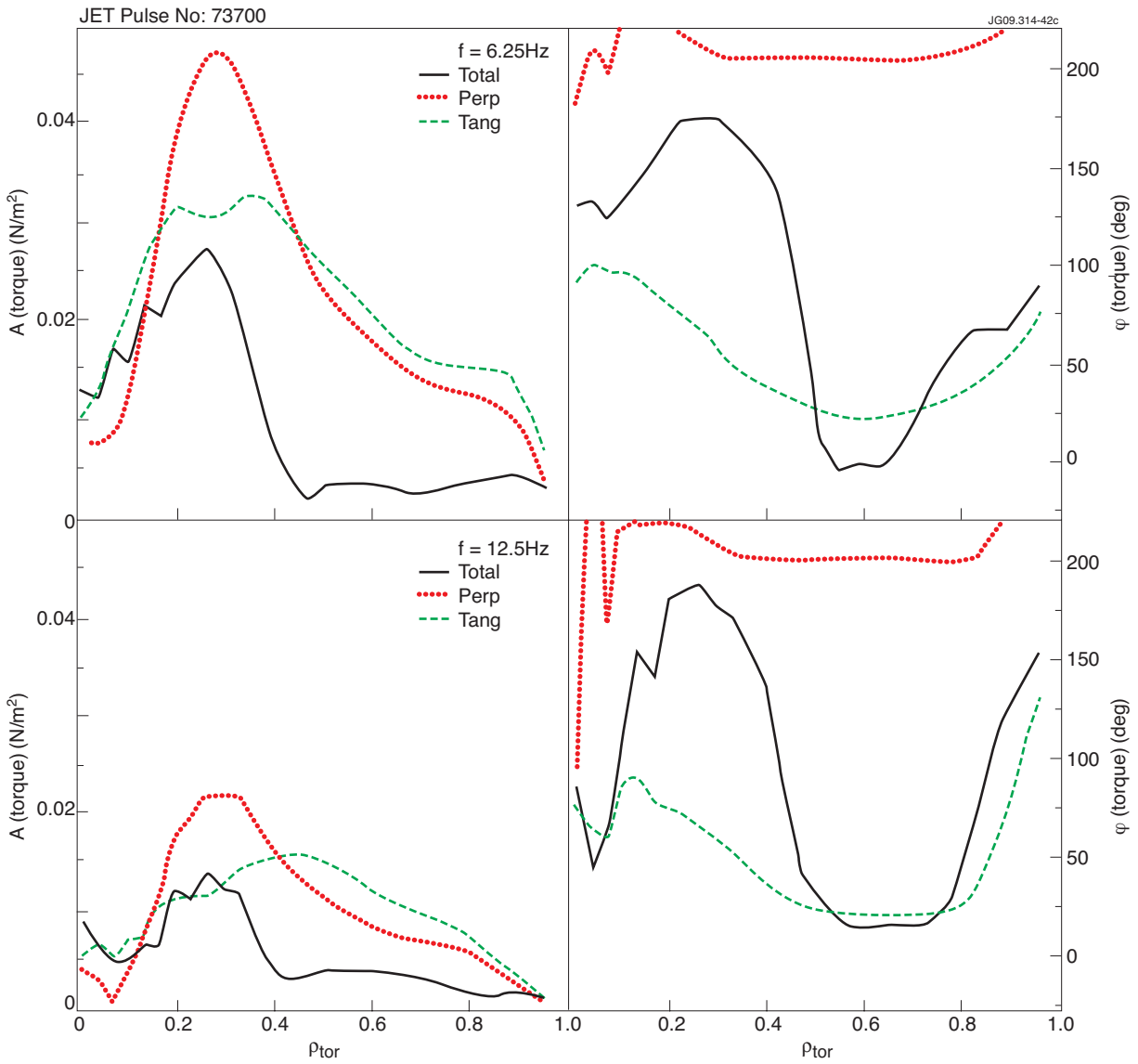

Figure 14: Radial profiles of A and φ of ASCOT calculated torque at 6.25 and 12.5Hz in Pulse No: 73700 (compensated), distinguishing tangential & perpendicular beam components.

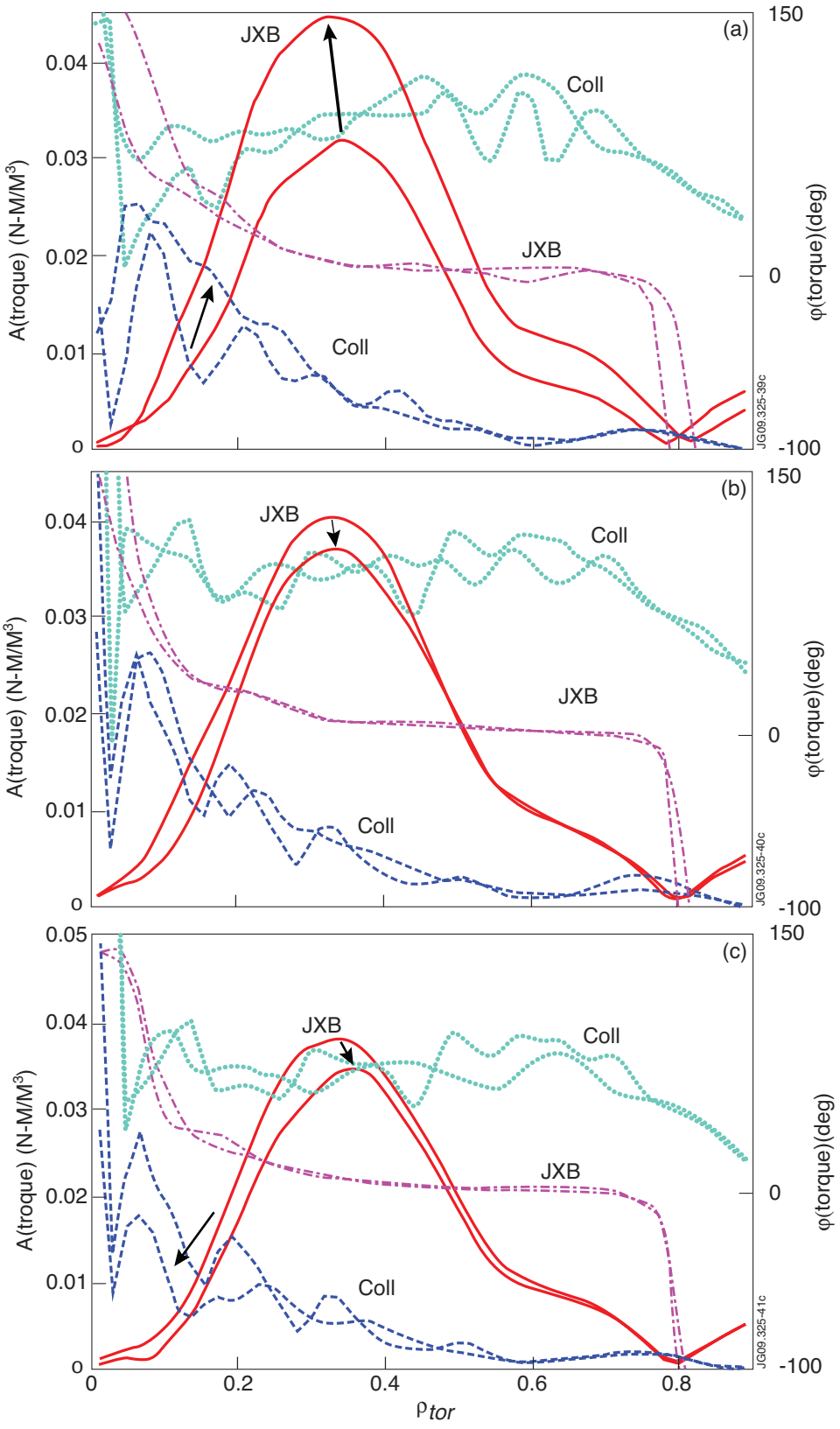

*Figure 15: Radial profiles of A and φ of TRANSP calculated torque at 8.33Hz in Pulse No:73701 with a) n_e varying between 0.8 and 1.2 of experimental value; b) T_e varying between 0.8 and 1.2 of experimental value; c) Z_{eff} varying between 1.9 and 1. Red full lines are A of **J×B** torque, blue dashed lines are A of collisional torque, violet dashed-dotted lines are φ of **J×B** torque and green dotted lines are φ of collisional torque. The arrows indicate the relevant changes due to parameter variation.*

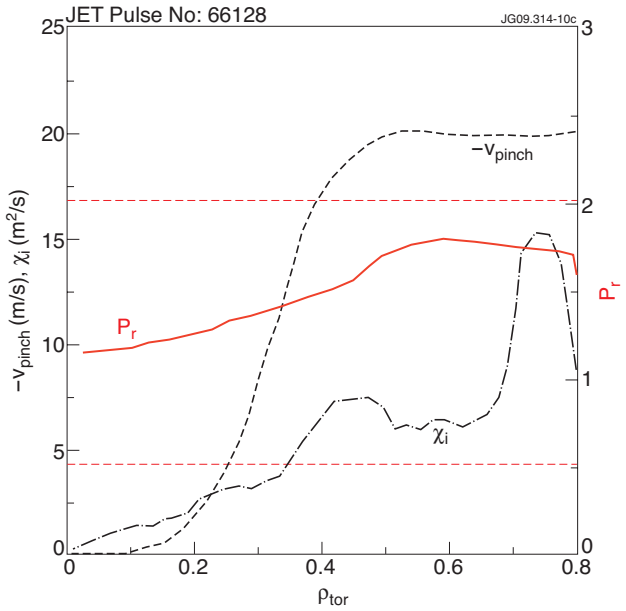

Figure 16: Radial profiles of $\chi_{i,}^{eff,}$ v_{pinch}, P_r used in the simulations of Pulse No: 66128 discussed in the text.

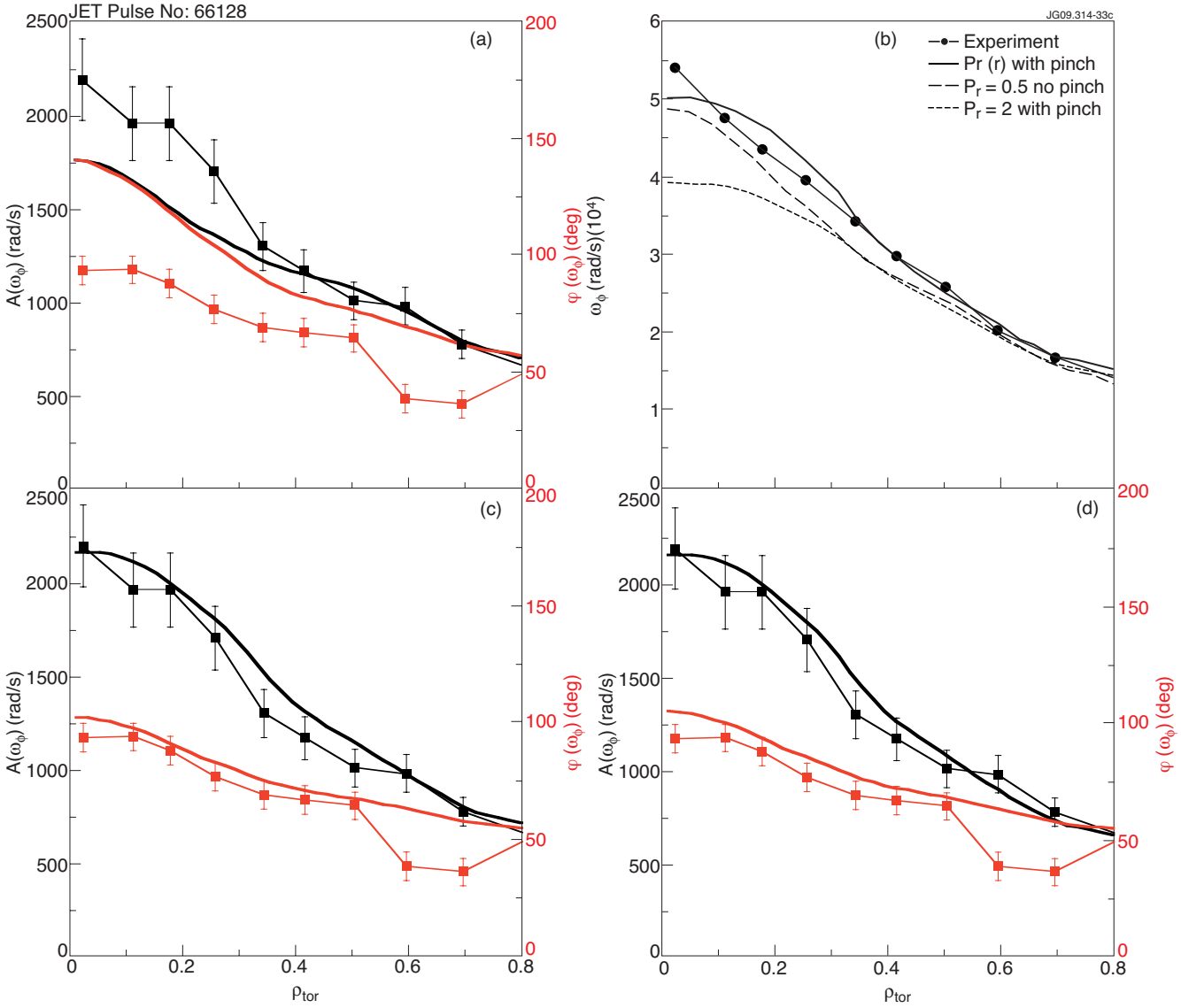

Figure 17: Radial profiles of experimental (dots) and simulated (lines) A and φ of ω_ϕ in Pulse No: 66128 using a) P_r = 0.5 and v_{pinch} = 0 m/s; c) P_r = 2 and vpinch as shown in Fig.16; d) a P_r profile increasing with radius (Fig.16) and vpinch as shown in Fig.16. In b) the radial profiles of experimental and angular rotation using the 3 different transport options are shown.

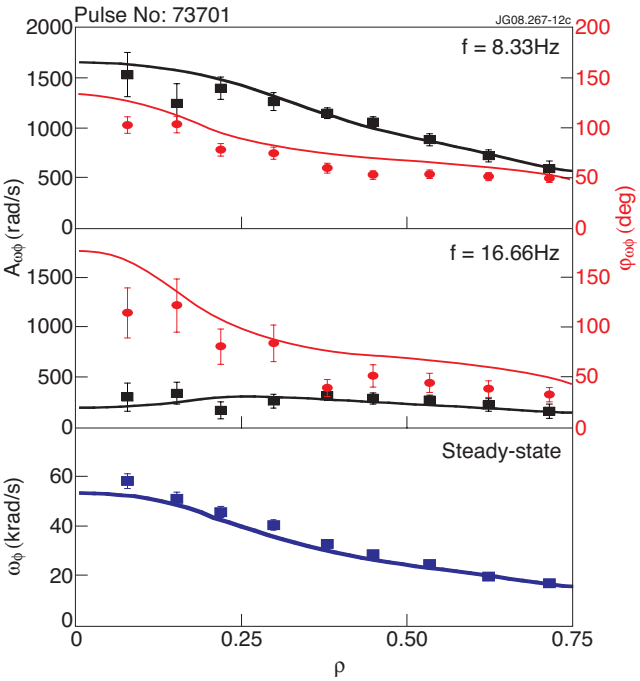

Figure 18: Radial profiles of experimental (dots) and simulated (lines) A and j of wf at two harmonics of the modulation frequency and steady-state ω_ϕ in Pulse No: 73701. The simulation best-fits to the data the P_r and vpinch profiles as shown in Fig.19.

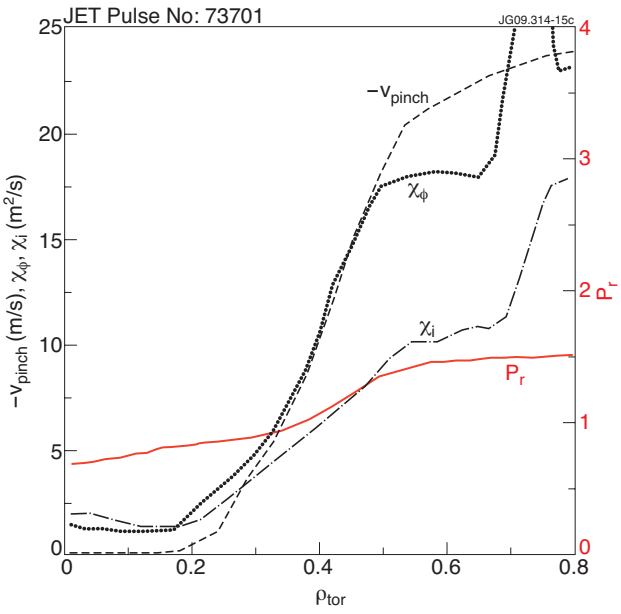

Figure 19: Radial profiles of χ_ϕ, χ_i, $-v_{pinch}$ and P_r from the empirical simulation of Pulse No: 73701.

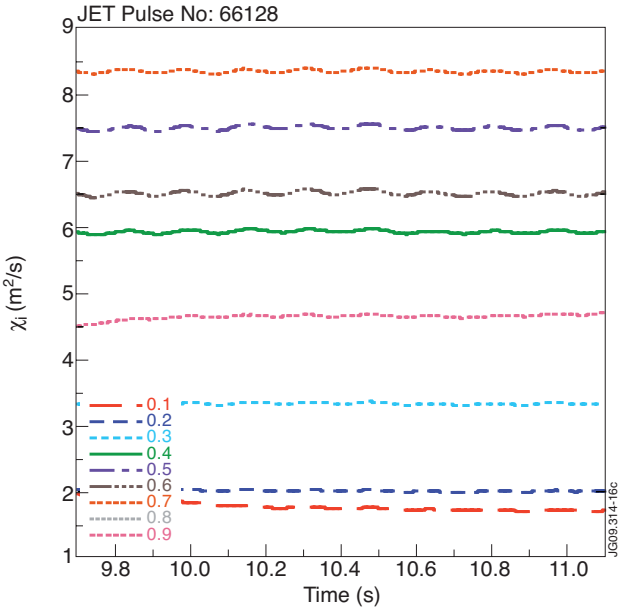

Figure 20: Time traces of χ_i and different radii as calculated for Pulse No: 66128 using the CGM model with typical values of ion threshold and stiffness derived from previous ion heat transport studies

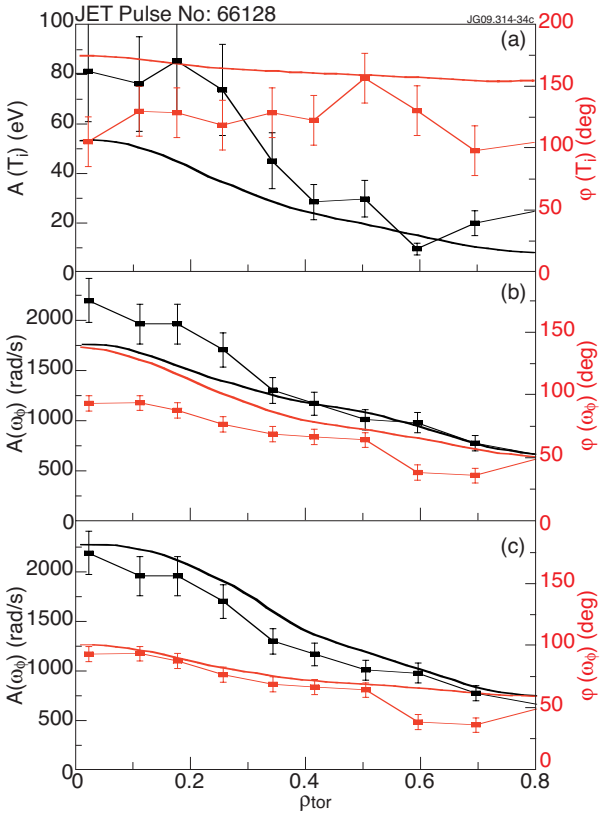

Figure 21: Radial profiles in Pulse No: 66128 of experimental (dots) and simulated (lines) A and φ of: a) T using χ_i from the CGM model; b) ω_ϕ using Pr=0.5 and v_{pinch} = 0 m/s and ci from the CGM model; c) ω_ϕ using the P_r profile increasing with radius (Fig.16) and vpinch as shown in Fig.16 and ci from the CGM model.

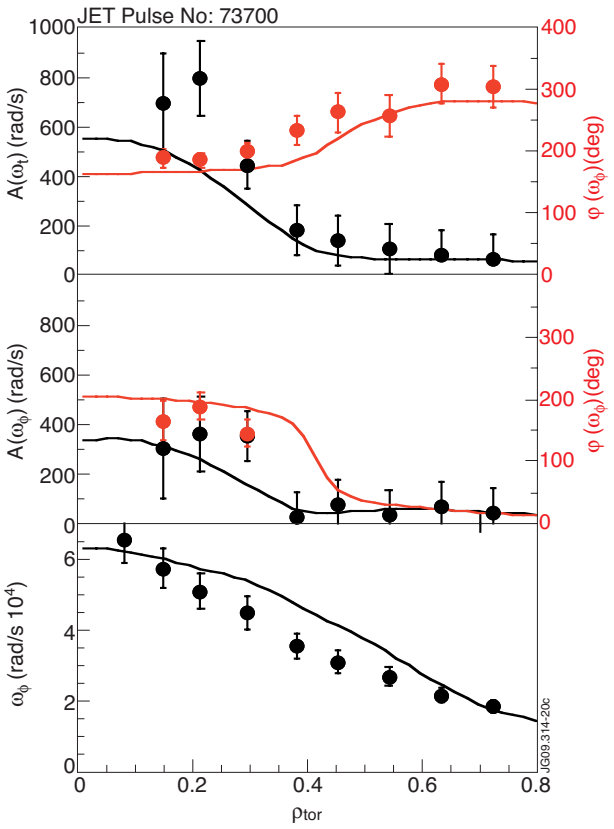

Figure 22: Radial profiles of experimental (dots) and simulated (lines) A and φ of φ_ϕ at two harmonics of the modulation frequency and steady-state φ_ϕ in Pulse No: 73700 (compensated case). The simulation best-fits to the data the P_r profile increasing with radius and the v_{pinch} profile as shown in Fig.23.

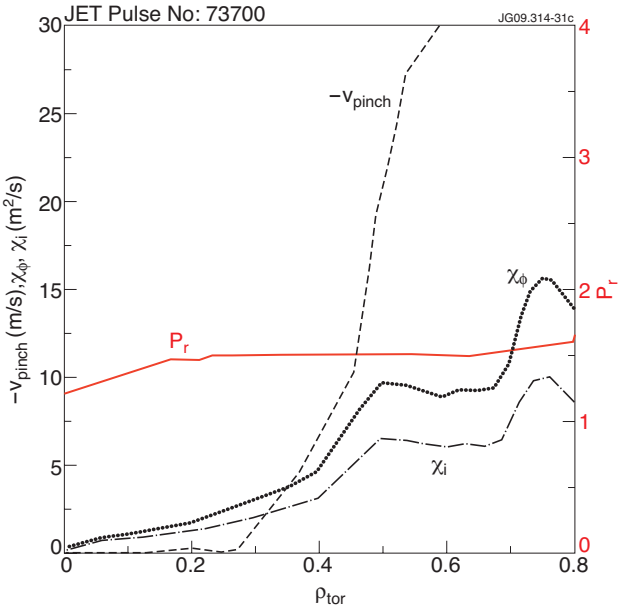

Figure 23: Radial profiles of χ_ϕ, χ_i, $-v_{pinch}$ and P_r from the empirical simulation of Pulse No: 73700.

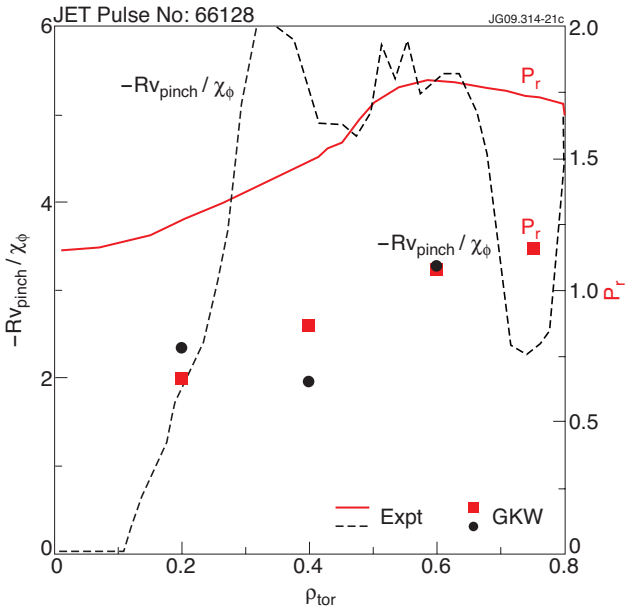

Figure 24: Comparison between experiment and linear gyro-kinetic simulations using GKW of the radial profile of P_r and $-Rv_{pinch}/\chi_\phi$ for Pulse No: 66128.

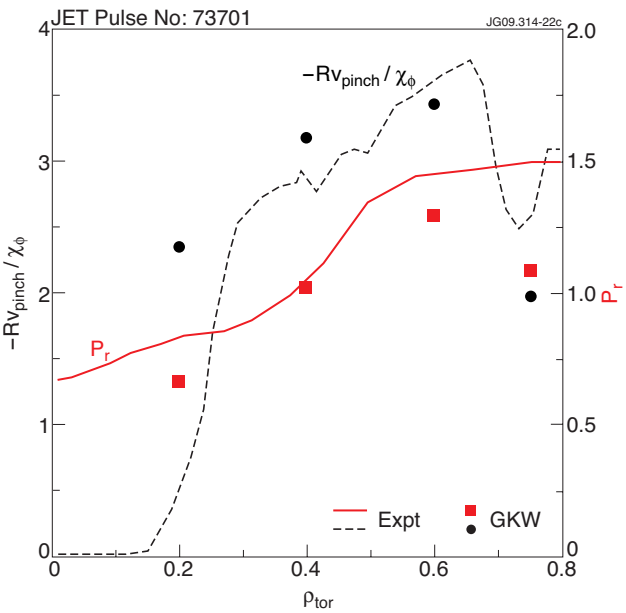

Figure 25: Comparison between experiment and linear gyro-kinetic simulations using GKW of the radial profile of P_r and $-Rv_{pinch}/\chi_\phi$ for Pulse No: 73701.

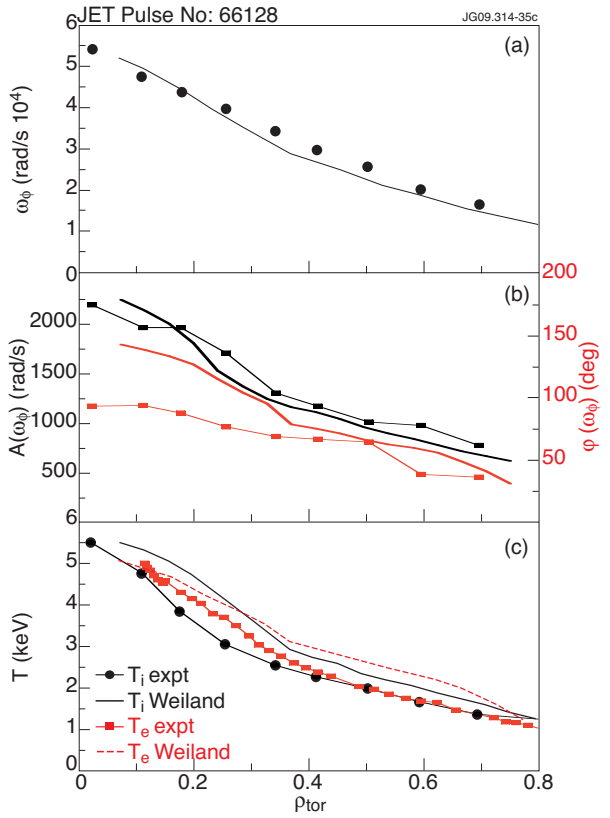

Figure 26: Radial profiles in Pulse No: 66128 of experimental (dots with line) and simulated (lines only) a) time-averaged steady-state ω_ϕ; b) A and φ of ω_ϕ; c) time-averaged steady-state T_i and T_e. The simulations are carried out using the Weiland model with T_i, T_e and ω_ϕ predicted and n_e fixed to the experimental profile.

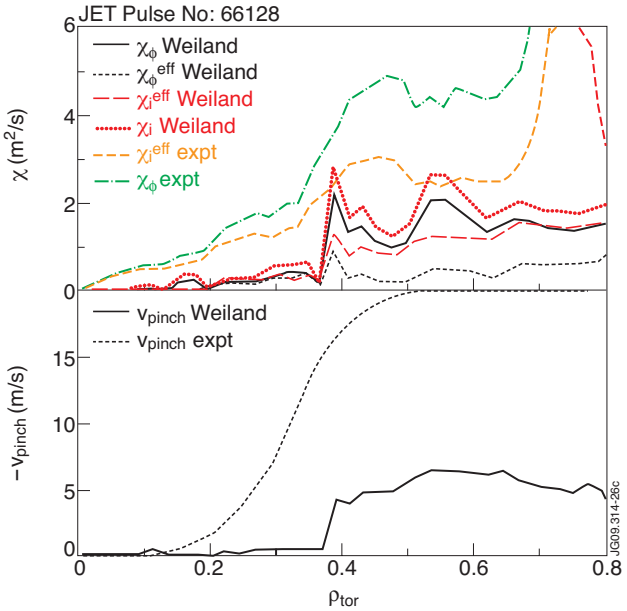

Figure 27: Radial profiles of turbulent χ_i (diagonal and effective), χ_φ (diagonal and effective) and momentum vpinch for the Weiland model simulation of Pulse No: 66128 shown in Fig.25, compared with profiles of effective χ_i (turbulent+neoclassical), diagonal χ_φ and v_{pinch} obtained by best-fitting experimental data.

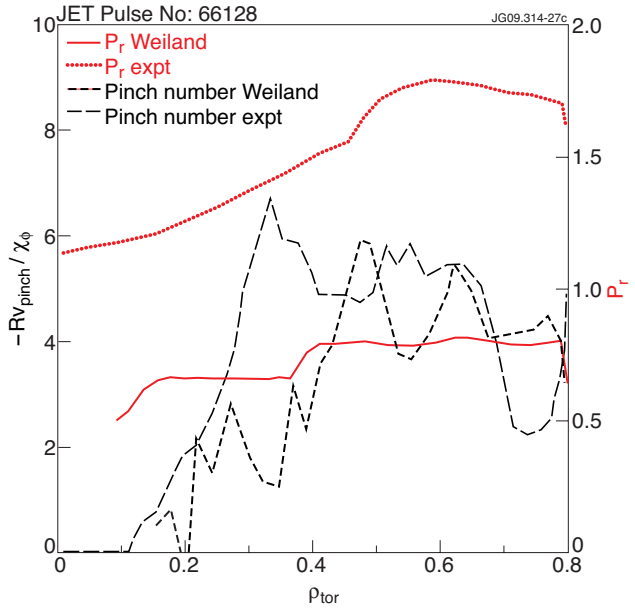

Figure 28: Comparison of radial profiles of Prandtl and pinch numbers from Weiland simulation and experiment for Pulse No: 66128.

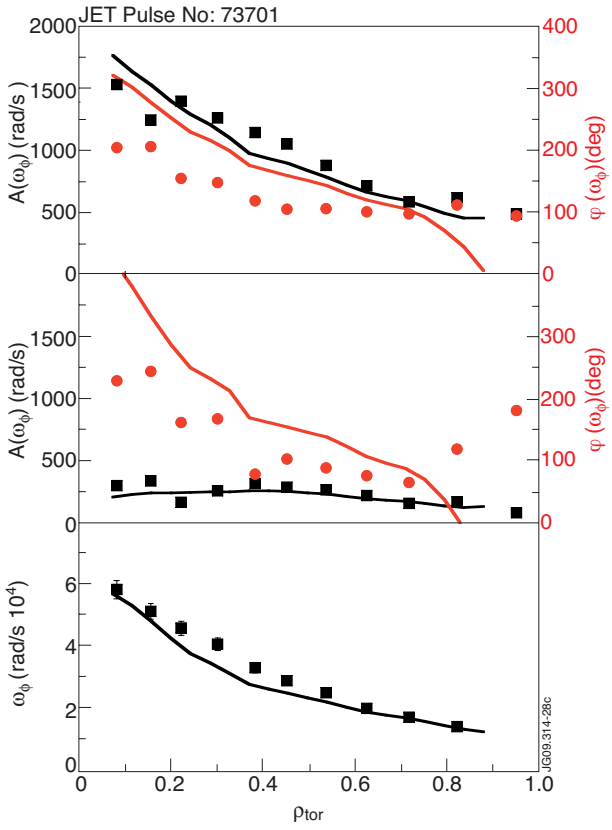

Figure 29: Radial profiles of experimental (dots) and simulated (lines) time-averaged $\omega_\phi(c)$ and its A and φ at 1st (a) and 2nd (b) harmonics in Pulse No: 73701 using the Weiland model with T_i, T_e and ω_ϕ predicted and n_e fixed to the experimental profile.

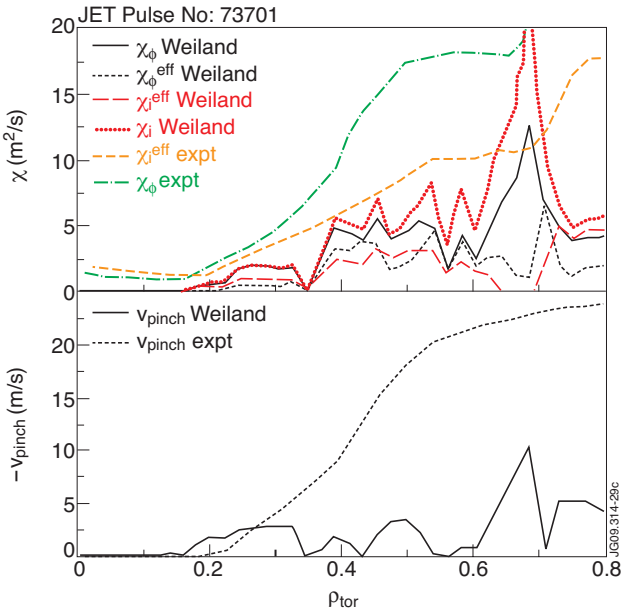

Figure 30: Radial profiles of turbulent χ_i (diagonal and effective), χ_φ (diagonal and effective) and momentum v_{pinch} for the Weiland model simulation of shot 73701 shown in Fig.29, compared with profiles of effective χ_i (turbulent+neoclassical), diagonal χ_φ and v_{pinch} obtained by best-fitting experimental data.

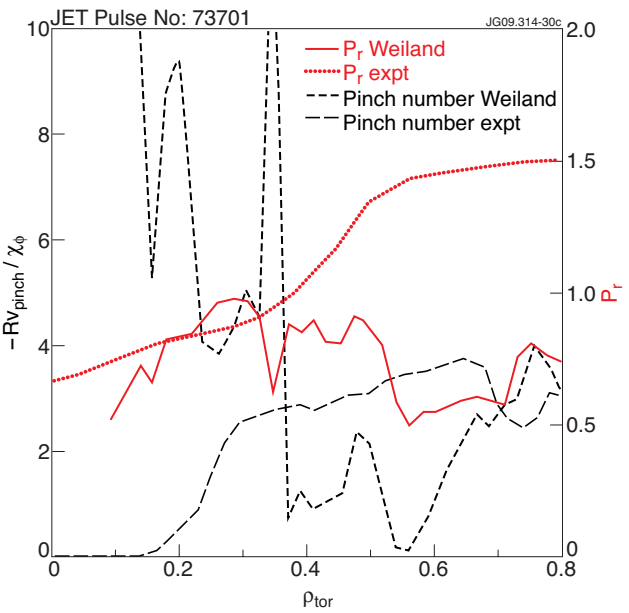

Figure 31: Comparison of radial profiles of Prandtl and pinch numbers from Weiland simulation and experiment for Pulse No: 73701.